# DEEPLY PENETRATING EVENTS IN THE EXTREMELY HIGH ENERGY COSMIC RAY FLUX

by

Bruce L. Emerson

A dissertation submitted to the faculty of
The University of Utah
in partial fulfillment of the requirements for the degree of

Doctor of Philosophy

Department of Physics

The University of Utah

August 1992

THE UNIVERSITY OF UTAH GRADUATE SCHOOL

# SUPERVISORY COMMITTEE APPROVAL

of a dissertation submitted by

Bruce L. Emerson

This dissertation has been read by each member of the following supervisory committee and by majority vote has been found to be satisfactory.

6-17-92 — Chair: Michael Salamon

6-17-92 — Pierre Sokolsky

6-17-92 — Haven Bergeson

6/17/92 — Richard Price

6/17/92 — Kuonan Liou

THE UNIVERSITY OF UTAH GRADUATE SCHOOL

# FINAL READING APPROVAL

To the Graduate Council of The University of Utah:

I have read the dissertation of Bruce L. Emerson in its final form and have found that (1) its format, citations, and bibliographic style are consistent and acceptable; (2) its illustrative materials including figures, tables, and charts are in place; and (3) the final manuscript is satisfactory to the Supervisory Committee and is ready for submission to the Graduate School.

7-1-92
Date

Michael Salamon
Chair, Supervisory Committee

Approved for the Major Department

P. Craig Taylor
Chair/Dean

Approved for the Graduate Council

B. Gale Dick
Dean of The Graduate School

# ABSTRACT

This dissertation will present the results of a search for deeply penetrating particles in the Extremely High Energy (EHE) (particle energy $\geq 10^{17}$eV) cosmic ray flux. The data are from the University of Utah Fly's Eye detector which is a unique detector for observing cosmic rays in this energy regime. Central to this search is the definition of a robust signature for deeply penetrating Extensive Air Showers (EAS) which is given as follows: *Candidate deeply penetrating events are those whose plane normal angle ($\theta_n$) is less than 18°*. The absence of events in the Fly's Eye data set meeting this criterion is examined in the context of models of astrophysical neutrino flux and charm production at EHE energies. The use of the calculations in this dissertation to test other models for the production of deeply penetrating extensive air showers is described where needed.

To Dawn and my family

# CONTENTS

# LIST OF TABLES

# ACKNOWLEDGMENTS

My profound thanks go out to the many friends and collegues without whose support this dissertation would not have been written. Your patience and support throughout my difficulties, both personal and professional, have made all of this possible. Particular thanks are due to Mike Salamon whose insight and comments kept the whole effort on track. In addition special thanks are due to Dawn and the rest of my family here and around the country for their cheerful and consistent support. To Tom McMahon, Mary Reed, Stefan Jeglinski, Matt Delong, Wayne Wingert, Brian Fick, Steve Corbató, Kevin Green, Barta Jones, along with the rest of the Fly's Eye and CASA collaborators, thanks for everything. A final thanks is due to the faculty of the Physics Department and the University of Utah for useful discussions having more to do with life than a degree and the many opportunities you gave me to teach your classes.

# CHAPTER 1

# INTRODUCTION

Observations of cosmic rays through their interactions with diverse detectors provide information pertinent to particle physics, cosmology, and astrophysics. What are they? Where do they originate? How do they get here? These are the basic questions common to all of cosmic ray astrophysics. The specific details necessarily vary with the energy of the cosmic rays being observed. This dissertation will present a search for deeply penetrating particles in the Extremely High Energy (EHE) (particle energy $\geq 10^{17}$eV) cosmic ray flux. Deeply penetrating particles are those that traverse an unusually large amount of atmospheric matter before interacting. The data are from the University of Utah Fly's Eye detector, which is a unique detector for observing cosmic rays in this energy regime. The implications of these measurements for particular questions from cosmology, astrophysics, and high-energy particle physics will be discussed.

The remainder of this introduction will be given over to a review of the properties of the EHE cosmic ray flux with a brief discussion of acceleration mechanisms, propagation, sources, and composition.

Chapter 2 describes the Fly's Eye experiment, what an Extensive Air Shower (EAS) is, how it is detected, and the parameterization of its characteristics. In addition, uncertainties and data contamination effects that are pertinent to deeply penetrating events are introduced. The FE aperture calculation is also defined and explained.

Chapter 3 is a review of deeply penetrating showers, explaining what they are and their what are their possible sources. The plausibility of each source in the context of the Fly's Eye experiment is examined qualitatively

In Chapter 4 the experimental signature of a deeply penetrating event is discussed. The fundamental question is how to distinguish a statistically unlikely, but otherwise uninteresting, hadronic shower from an event that is truely deeply penetrating. To discriminate against hadronic showers an event parameter examined and a requirement is defined such that an event meeting this requirement is not a standard hadronic shower to some confidence level. The chapter closes with a discussion of the implementation of this requirement

The results of searching the Fly's Eye data base of monocular reconstructed events for those that meet the deeply penetrating event requirement discussed in Chapter 4 are given in Chapter 5. Effects that would lead to contamination of the data set with spurious events are evaluated. No events are found that meet the requirement for deeply penetrating EAS.

The remainder of the dissertation is devoted to discussing the implications of the absence of deeply penetrating events for particular models from cosmology and high energy particle physics. Chapter 6 addresses the consistency of the absence of events with two current models of the production of astrophysical neutrinos. The methodology for doing consistency checks with other neutrino flux models is also presented.

Chapter 7 considers the consistency of the absence of deeply penetrating events with current expectations for the production of charmed matter (i.e., hadrons with charm quark component) in EAS from EHE cosmic rays. Because the energy regime for EAS from EHE cosmic rays is well above that of any current land-based particle accelerators, the parameters for modeling charm production must be extrapolated from existing data. Details of the charm propagation model are presented along with points where additional theoretical information is needed to refine the model.

Due to the fact that no candidate events are observed, the question of how to differentiate neutrino induced events from charm events never arises. In Chapter

8, a method for potentially distinguishing these two types of events is presented.

Finally, Chapter 9 summarizes the work and results of this dissertation.

## 1.1 Extremely High Energy Cosmic Rays

Extemely High Energy (EHE) cosmic rays are defined to be those whose energy is greater than 0.1 EeV (EeV = $10^{18}$eV). Historically this energy regime has also been known as the Ultra High Energy (UHE) regime. EHE cosmic rays can be characterized by both the physics associated with them and the methods for their detection. In the former case, acceleration mechanisms to boost particles to these enormous energies and the physics of cosmic ray propagation through the intervening media constitute the principal areas of investigation. In the latter case, the detection of EHE cosmic rays through the interaction of the associated Extensive Air Shower (EAS) with ground arrays, underground muon arrays, and atmospheric scintillation are currently the only means for generating acceptable data rates. This section will be devoted to an introduction to the physics of EHE cosmic rays while the experimental details of detection of these particles will be left to the following chapter.

By convention, what is meant by the cosmic ray spectrum is the differential flux of particles, dN/dE ($m^{-2} \cdot sr^{-1} \cdot s^{-1} \cdot GeV^{-1}$). For energies above 10 GeV/particle the cosmic ray spectrum follows an inverse power law (Figure 1.1) of the form dN/dE $\propto E^{-(\gamma+1)}$ in a common parameterization. Note the change in spectral slope just above $10^{15}$eV known as the knee of the spectrum. There is also a much-debated flattening of the spectrum around 10 EeV referred to as the ankle. Besides these anatomical points, the important features are the simple power law dependence at energies above and below the knee and the consistency of the results from several independent experiments. The energy dependence below $10^{15}$ eV is $E^{-2.76\pm0.09}$[20] while at energies above $10^{16}$ eV it is $E^{-3.03\pm0.03}$[50]. The consistency of this result

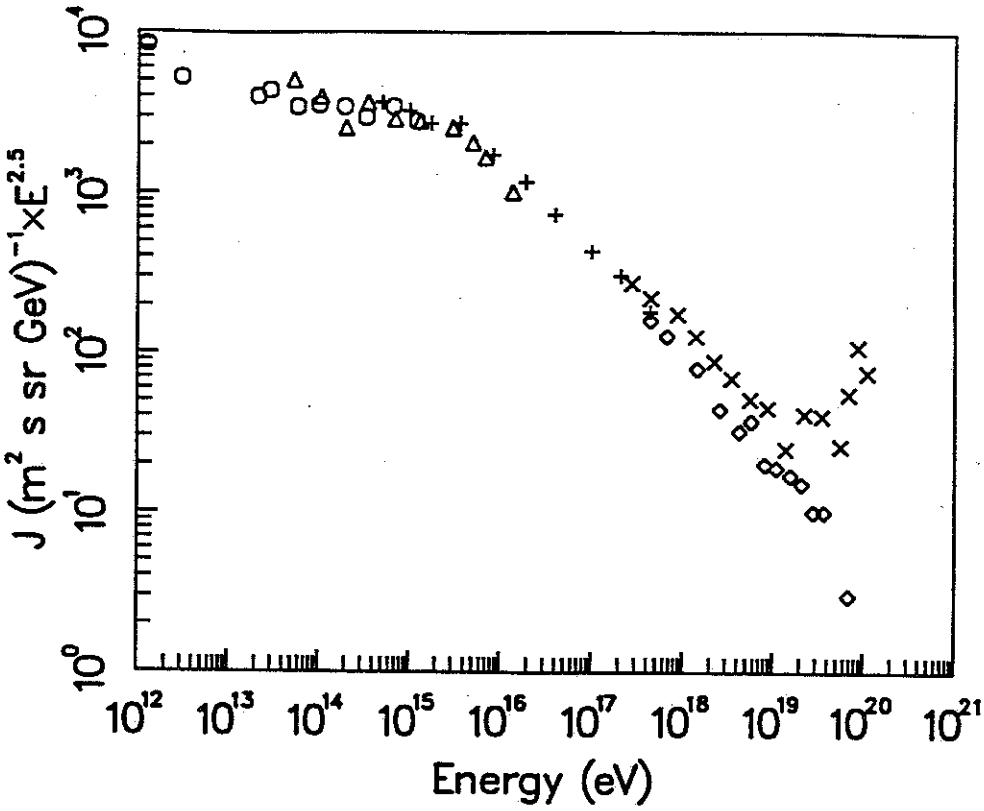


Figure 1.1. Differential cosmic ray spectrum

over many orders of magnitude in energy is an important constraint on models for the production of high energy cosmic rays.

The details of this spectrum provide information and constraints for models of cosmic ray propagation, proposed acceleration mechanisms, cosmology, and source models. Although there remain many questions, there is a certain consensus about the principal features of the spectrum and the physics that underlies its form. I will now review the current views regarding acceleration mechanisms, sources, propagation, and composition of cosmic rays that give rise to the observed spectrum. It is important to note that all of these topics are strongly interrelated when used to interpret the empirical data. The choice of proposed acceleration mechanism affects the probable source environments, which in turn set limits on the possible propagation paths. These paths affect the composition expected for the spectrum. It is often possible to develop a number of different plausible models to explain the

observed data. This is an essential feature of the EHE cosmic ray field and is the result of the limited number of clear results.

### 1.1.1 Acceleration Mechanisms

Because the charge-neutral component of the cosmic ray flux is less than $5 \cdot 10^{-4}$ [69] of the total flux, cosmic rays are taken to be fully ionized atomic nuclei for the purposes of this discussion. These can be accelerated by a variety of electrodynamical processes. In addition to the power law dependence of the spectrum another important feature of EHE cosmic rays is the relatively small energy density of this portion of the spectrum. Assuming EHE cosmic rays are confined to the region of the galactic halo the power needed to supply these cosmic rays is on the order of $2 \cdot 10^{36}$ ergs/s for cosmic rays with energies greater than $10^{17}$ eV. This is substantially less than the $3 \cdot 10^{42}$ ergs/s provided by supernovae in the galaxy. This means that a small number of very energetic sources could produce the observed flux of EHE cosmic rays. Because very few sources are needed to explain the data even unlikely mechanisms for particle acceleration merit examination.

Statistical acceleration is a very attractive mechanism due to its natural production of a power law spectrum. These processes involve a large number of small, sequential accelerations where a power law spectrum is obtained in the following way (after the method of Gaisser [46, pp 149]). Let $E_0$ be the initial energy of the particle and $\epsilon E$ the increase in energy due to a single interation of the acceleration process. The energy of the particle after $n$ iterations is then

$$E_n = E_0 \cdot (1 + \epsilon)^n, \tag{1.1}$$

which can be rearranged to give

$$n = \frac{ln(E_n/E_0)}{ln(1 + \epsilon)}. \tag{1.2}$$

If the probability of the particle escaping from the acceleration region is $P_{esc}$ then $(1\text{-}P_{esc})^n$ is the probability that the particle experiences $n$ accelerations. It should be noted that for plausible scenarios both $\epsilon$ and $P_{esc}$ will be small. Given a number of particles with energy $E_0$ injected into the acceleration region the number of particles ($N_{E_n}$) with terminal energy greater than $E_n$ has the following dependence on $P_{esc}$;

$$N_{E_n} \propto \sum_{k=n}^{\infty}(1-P_{esc})^k = \frac{(1-P_{esc})^n}{P_{esc}} \tag{1.3}$$

Combining 1.2 and 1.3 yields

$$N_{E_n} \propto \frac{1}{P_{esc}}\left(\frac{E_n}{E_0}\right)^{-\gamma} \tag{1.4}$$

where

$$\gamma = \frac{-ln(1-P_{esc})}{ln(1+\epsilon)} \approx \frac{P_{esc}}{\epsilon} \tag{1.5}$$

Equation 1.4 is a power law spectrum for the integral flux of particles above some energy leading to a $-(1+\gamma)$ energy dependence in the differential spectrum. An upper limit on the energy attainable through such a process can be estimated first noting that there will be a maximum number of accelerations that depends on the residence time of the particle in the acceleration region. If $T_{res}$ is the residence time in the acceleration region and $T_n$ is the mean time between accelerations then the power law spectrum will roll off at a characteristic energy given by

$$E_{roll} = E_0 \cdot (1+\epsilon)^{T_{res}/T_n} \tag{1.6}$$

The residence time can be given by the lifetime of the acceleration mechanism as in the case of supernova shocks or by the age of the particles being accelerated.

Fermi acceleration [42] is the classic statistical acceleration process in the field of cosmic rays. The theory (after the method of Gaisser [46, pp 151]) considers the effect of encounters between individual particles and regions of magnetic turbulence (see Figures 1.2 and 1.3). A relativistic particle with energy $E_0$ enters the magnetic

cloud and is isotropised through collisionless scattering. Collisionless scatterings are interactions that involve no energy loss. The energy of the cosmic ray particle in the rest frame of the moving plasma is given by

$$E_1 = \gamma E_0(1 - \bar{\beta} \cdot \hat{n_i}) \tag{1.7}$$

where $\gamma$ and $\beta$ are the standard relativistic factors for the plasma cloud with respect to the lab frame and $\hat{n_i}$ is the unit vector in the direction of the incident particle motion. When the particle escapes from the cloud in the $\hat{n_e}$ direction, it now has energy in the lab frame given by

$$E_2 = \gamma E_1(1 + \bar{\beta} \cdot \hat{n_e}) \tag{1.8}$$

which leads to the following expression for the net energy change in the lab frame.

$$\Delta E/E_0 = (1 - \beta cos\theta_i - \beta cos\theta_i cos\theta_e + \beta cos\theta_e)/(1 - \beta^2) - 1 \tag{1.9}$$

In this expression $\bar{\beta} \cdot \hat{n_i}$ has been replaced by $\beta cos\theta_i$ and $\bar{\beta} \cdot \hat{n_e}$ has been replaced by $\beta cos\theta_e$. Two distinct cases need to be considered at this point. In the case of localized plasmas the particle can exit the cloud in any direction as can be seen in Figure 1.2. Planar shock fronts can only be exited through the shock front as shown in Figure 1.3. The assumption of a planar shock front is valid in cases where the mean free path of the particle is much less than the radius of curvature of the shock. In the case of many shock models this is a reasonable assumption.

To estimate the average energy gain in each case, the average over $cos\theta_e$ is taken and Equation 1.9 reduces to

$$< \Delta E/E_0 >= (1 - \beta cos\theta_i)/(1 - \beta^2) - 1 \tag{1.10}$$

for localized plasmas and to

$$< \Delta E/E_0 >= (1 - \beta cos\theta_i + 2/3\beta - 2/3\beta^2 cos\theta_i)/(1 - \beta^2) - 1 \tag{1.11}$$

for shock fronts. The same effect comes into play when considering the allowed geometries for $\theta_i$. Averaging over $\theta_i$ in each case, substituting into the previous

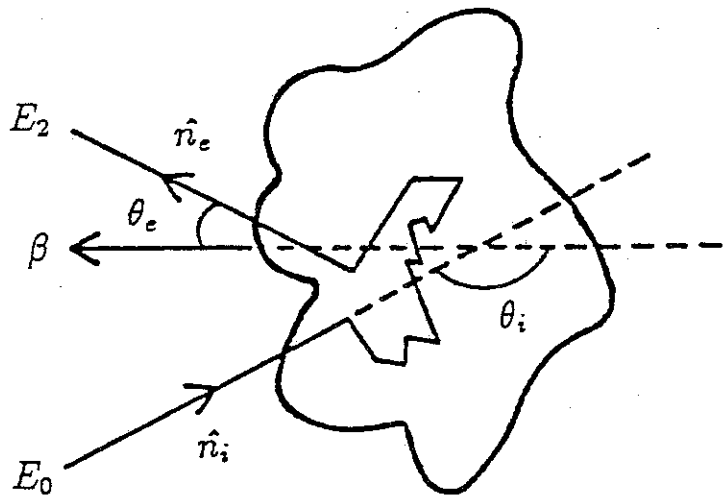


Figure 1.2. General Fermi shock acceleration geometry

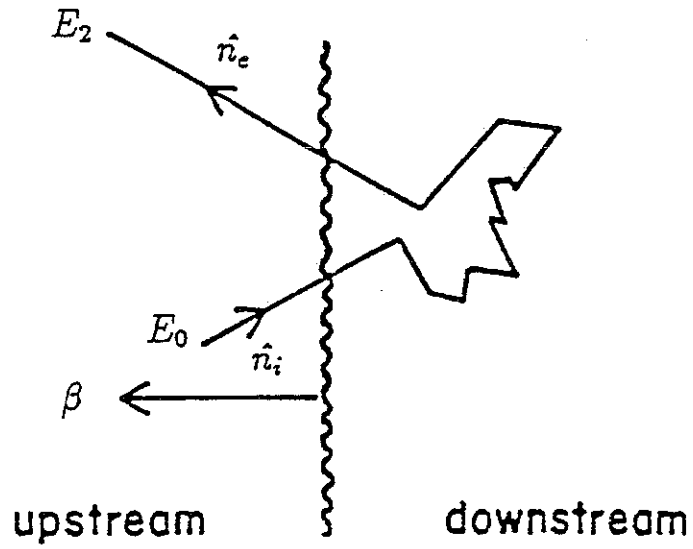


Figure 1.3. Planar shock acceleration geometry

equations, and noting that $\Delta E/E_0$ is just the fractional increase in particle energy $\epsilon$ previously defined, it is found that

$$\epsilon \sim (4/3)\beta^2 \tag{1.12}$$

for localized plasmas and

$$\epsilon \sim (4/3)\beta \tag{1.13}$$

for the shock front case. These two cases are respectively known as 2nd order and 1st order Fermi acceleration. For particles with the same residence time in a particular acceleration environment, 1st order Fermi acceleration will lead to higher energy particles than if the accleration mechanism is 2nd order. For this reason many of the models proposed to accelerate cosmic rays to EHE energies involve 1st order Fermi accleration at strong shock fronts.

A variety of acceleration mechanisms are associated with compact objects such as pulsars, neutron stars, and Active Galactic Nuclei (AGN's) [46, 52, 32]. As an example, consider the model of Gaisser *et al.*[45]. The model considers a neutron star at the center of the expanding shell of supernova ejecta as the central engine of an EHE particle accelerator. It is assumed that the neutron star is rapidly rotating and has a strong, $\sim 10^{12}$G, magnetic field. In a vacuum such a pulsar would lose energy through magnetic dipole radiation. In this case the surrounding plasma is assumed to be of a density such that the plasma frequency is larger than the pulsar frequency. Under these conditions, the electromagnetic wave will not propagate through the plasma but will drive a relativistic wind of particles. This wind will be confined by the surrounding ejecta producing a standing shock. In an earlier paper [44] Gaisser *et al.* considered first-order Fermi acceleration at this shock front. They calculated that for a 10 ms pulsar with a $10^{12}$G surface field that protons could be accelerated to $2 \cdot 10^{16}$eV. For a 1 ms pulsar with the same magnetic field the limit would rise to $2 \cdot 10^{18}$eV particles.

Another model of EHE particle acceleration is due to Biermann and Stritmatter [13] and considers shock acceleration in radio jets of AGN's. The motivation was an attempt to explain the infrared cutoff in the synchrotron spectrum. A shock is formed where the flux from the AGN encounters the intergalactic medium. Cosmic ray nuclei are accelerated at this shock with the maximum energy being limited by synchrotron and photon-interaction losses. This model of cosmic ray accleration predicts that protons could be accelerated to energies on the order of $10^{21}$eV.

An EHE acceleration model due to Jokipii and Morfill [62] suggests that there exists the galactic analog of the solar wind termination shock. Such a shock, created by the outflowing plasma and cosmic rays, is postulated to form at a distance of roughly 3 kpc from the galactic disc. The shock is taken to be strong with a compression ratio of nearly 4. The spiraling galactic magnetic field results in the drift of particles along the shock front. Particles accelerated to energies of $10^{15}$eV by supernova shock acceleration are assumed to form the injection spectrum. Calculations in this model indicate that particle energies of $10^{19} - 10^{20}$eV can be reached through 1st order Fermi shock acceleration in this environment. The total timescale for this acceleration process is 7-10·$10^9$ yr. An acceleration mechanism that does not involve shock acceleration is the disk dynamo. In this model, described by Chanmugam and Brecher [26], the important feature is the interaction of the rotating accretion disk with the magnetic field of the neutron star. The accreting plasma gives rise to a $v \times$B electric field across the disk. The potential difference across the disk is given by

$$V = -300((GM)^{-1/2}/c)B_z(r_1)r_1^{1/2}ln(r_2/r_1) \qquad (1.14)$$

where $r_1$ and $r_2$ are the inner and out radii of the accretion disk. For a dipole magnetic field whose axis is parallel to the rotation axis, $r_1$ is the magnetospheric, or Alfven, radius given by

$$r_1 = 1.8 \cdot 10^8 B_{12}^{4/7} R_6^{10/7} (M/M_\odot)^{1/7} L_{38}^{-2/7} cm \quad (1.15)$$

where $B_{12}$ is the suface magnetic field in units of $10^{12}$ Gauss, $R_6$ is the radius of the neutron star in units of $10^6$ cm, and $L_{38}$ is the total accretion luminosity in units of $10^{38}$ ergs/s. An interesting feature of this model is that the largest potentials are found for the smallest surface fields at the neutron star. This is due to the coupling between $r_1$ and the magnitude of the surface magnetic field. Taking a surface field of $10^8$ Gauss, $M = 1 \cdot M_\odot$, and an accretion luminosity equal to the Eddington luminosity, the maximum potential given by the above expression is $2 \cdot 10^{17}$eV. The authors also speculate that if the magnetic energy were discharged in bursts due to plasma jets then this limit might increase by as much as 100.

### 1.1.2 Propagation

The propagation of cosmic rays from their sources through the intervening media is an important question in the study of cosmic rays of all energies. At EHE energies, the propagation of cosmic rays to the local region of the galaxy is intertwined with questions about the galactic or extragalactic sources of these particles. Different propagation environments must be considered if the sources are not in the galaxy. In either case the age of the cosmic rays is a related issue. All of these questions, and others, have been effectively addressed through careful measurements of the relative abundances of the different nuclei in the cosmic ray spectrum at energies below $10^{14}$ eV. Due to the low particle flux and the experimental techniques for detecting EHE cosmic rays detailed measurements of the composition of the EHE flux are not currently possible. As a result, the knowledge of the propagation environment of EHE energies is much less specific.

Below $10^{14}$ eV atomic abundance measurements [90] and isotopic ratio measurements [73] indicate that such cosmic rays propagate primarily in the galactic halo. At EHE energies, where there are no measurements of the path lengths or

age of cosmic rays, it is thought that such particles propagate almost exclusively through the intergalactic medium. Because of the absence of measurements the propagation environment of EHE cosmic rays in models of the cosmic ray spectrum is only mildly constrained.

No discussion of cosmic ray propagation would be complete without the inclusion of the much sought after Greisen-Zatsepin cut-off of the EHE spectrum. Soon after the discovery [78] of the 2.7° blackbody radiation that permeates, the universe both Greisen [51] and Zatsepin and Kuz'min [94] independently realized that this would have a dramatic effect on the propagation of extragalactic cosmic rays. Through photomeson production [86] and photodissociation [81] processes cosmic ray nuclei with energies greater than $\sim 10^{20}$eV have a significant cross section for interaction with the blackbody photons. Various authors have calculated the effect of this interaction cross section on the EHE cosmic ray flux. The results indicate that if the sources of these particles are within 10 Mpc there will be no noticeable effect on the spectrum irrespective of the composition. For sources more distant than 10 Mpc, an iron rich cosmic ray flux should show a noticable steepening at around $10^{20}$eV due to photodissociation. A proton rich flux would show no effects from photomeson production unless the sources were more distant than 100 Mpc. Despite the fact that there is no compelling evidence that EHE cosmic ray sources are predominantly more distant than 10 Mpc, the steepening or cutoff of the spectrum around $10^{20}$eV has been much sought after [6, 22, 66, 50, 64]. The Fly's Eye data set contains no events above $10^{20}$ eV [7]. This is inconsistent, at the 98% C.L. with the four events expected for the current data set in the absence of a GZ cutoff of the spectrum. This suggests that there is indeed a steepening, or cutoff, of the cosmic rays spectrum in this energy regime. Other EHE detectors see no evidence for a cutoff of the cosmic ray spectrum at energies below $10^{20}$ eV [66] but the statistics in all experiments are still poor.

### 1.1.3 Sources

For a number of years, much experimental effort has been directed toward the search for point sources at EHE energies. Searching for point sources in the high energy cosmic ray flux is normally made impractical by gyromagnetic effects that alter the direction of particle motion. At particle energies above $10^{19}$eV, the gyroradius effect becomes negligible in the context of galactic sources. The magnitude of this effect for extragalactic sources of EHE particles is unclear due to uncertainties about the form of the intergalactic magnetic field. At this energy, our ability to observe sources is also hampered by the miniscule flux. The integrated flux above $10^{19}$eV is a few per km$^2$ per year. In general, this means that unless there is a significant EHE neutral flux, point sources will be quite difficult to detect. To date a number of point sources of TeV and PeV $\gamma$'s have been found [80]. These include Cygnus X-3, Hercules X-1 and the Crab pulsar. There is some indication that Cygnus X-3 is also a point source at EHE energies [23]. Because only neutral particles propagate directly from the source, in the absence of collisions, the challenge is to discriminate between charged and neutral particles in the cosmic ray flux in order to enhance the signal to noise ratio.

Questions regarding diffuse galactic sources can be addressed through measurements of the anisotropy of cosmic rays. Is there an enhancement of the cosmic ray flux from the direction of the galactic disk or core? Is there an enhancement from the direction opposite the galactic core? Measurements like this can address the question of whether the EHE sources are primarily in the galactic disc. To date measurements of EHE anisotropy by the Fly's Eye find no significant deviations from an isotropic flux [34]. This is not a significant constraint on source models because uncertainties about specific properties of the galactic environment lead to detectable anisotropy in under some assumptions and complete isotropy under others.

In principle, the existence of a cutoff of the EHE spectrum around $10^{20}$ eV would indicate that cosmic rays in this energy regime are produced in very distant sources. If the EHE flux consists primarily of protons, such a cutoff indicates that the sources are more distant than 100 Mpc. Even an iron rich flux would indicate sources on a distance scale of 10 Mpc if a cutoff exists. As previously discussed, current measurements [50] show some evidence of such a cutoff.

### 1.1.4 Composition

Because some models of EHE particle acceleration and sources are dependent on the Z of the nuclei, the elemental composition of cosmic rays is important to understanding their origin. The ratio of nuclei formed by spallation to heavy parent nuclei is an important indicator of the amount of material traversed by the cosmic rays. This is due to the spallation of heavy nuclei into lighter ones. The abundance of protons in the cosmic ray flux relative to heavier nuclei may set constraints on the proposed sources and their attendent acceleration mechanisms. Up to 30 TeV, where the flux is large, the composition of the cosmic ray flux is known with reasonable accuracy [90]. Because direct detection of cosmic rays is essential to an accurate determination of the composition, the low flux at higher energies makes it unlikely that this measurement will be extended above the 100 TeV range in the near future. At energies above 1 PeV, where indirect detection of cosmic rays is the norm, the determination of the composition is necessarily less precise. The analysis of the Fly's Eye data in this context is typical [24]. In models of Extensive Air Shower development showers initiated by heavy nuclei have shallower depths of maximum and less fluctuation about that maximum than do proton initiated showers. This can be understood qualitatively by considering heavy nuclei to be the superposition of an appropriate number of proton showers where the energy of each constituent shower is $E_{primary}/A_{nuclei}$. In this first order approximation, the fluctuations of

the protonic subshowers will smooth each other out, leading to less fluctuation in the total shower development. Because higher energy particles yield showers which take longer to develop to their maximum, an experimentally measured effect known as the elongation rate, showers initiated by the superposition of lower energy particles will reach their maximum size more quickly. An EAS initiated by an iron nuclei will typically reach its maximum size 100 g/cm$^2$ shallower than a proton of equal energy. This difference of 100 g/cm$^2$ is at the level of the resolution of the FE detector and limits the ability of the experiment to distinguish between heavy and light nuclei. For this reason the strongest statement about the composition of cosmic rays at EHE energies that is supported by the data is that the flux is not dominated by either protons or heavy nuclei [25]. Similiar results have been found at PeV energies. This conclusion is important for models of EHE particle acceleration like the galactic wind termination shock model of Jokipii *et al.*[62]. In this model heavy nuclei like iron are accelerated more effectively leading to an expectation of an iron dominated composition at EHE energies. Similiarly, cosmic string models for the production of EHE particles would yield only protons. This appears to be inconsistent with the present data. As can be seen, even general knowledge of the composition of EHE cosmic rays can provide useful constaints on some models.

### 1.1.5 Summary

The principal features of EHE cosmic rays can be summarized as follows: The differential flux of EHE cosmic rays has a constant power law dependence $\propto E^{-3.03\pm0.03}$ between $10^{16}$eV and $5 \cdot 10^{18}$eV. Above $5 \cdot 10^{18}$ there is some indication of for a flattening and/or a cutoff of the spectrum. The apparent cutoff is not inconsistent with the mechanism proposed independently by Greisen and Zatsepin. There exist plausible models for the acceleration of particles to EHE energies in the literature.

# CHAPTER 2

# DATA AQUISITION

The data for this dissertation are from the Fly's Eye (FE) detector, which has been extensively described elsewhere [50, 8]. For this reason, only a brief overview of the experiment will be given here. Those specific aspects of detector performance that affect the data pertinent to this dissertation will be discussed in more detail.

## 2.1 Extensive Air Showers

An Extensive Air Shower (EAS) is the result of the interaction of a single cosmic ray particle with the atmosphere it is traversing. Qualitatively it begins with the initial interaction of the cosmic ray particle with the earth's atmosphere. A number of secondary particles are produced in this interaction. These secondaries themselves interact with the atmosphere and produce further secondary particles. The number of particles in this cascade increases rapidly until the point where individual particle energies are low enough that energy loss mechanisms dominate particle production processes. The point at which the number of particles in the cascade peaks is known as the shower maximum. From this point on the number of particles diminishes until all are absorbed by the medium. For EAS initiated by cosmic ray nuclei there are three principal components to the shower.

The core of the shower is the hadronic component, which contains the hadronic products of the initial cosmic ray interaction as well as those hadrons from subsequent interactions of the shower particles with the atmosphere. This core remains localized near the axis of the shower due to the small tranverse momentum of the particles relative to their energy. The hadronic component of the shower

grows through fragmentation of target nuclei, generation of secondary baryons. and regeneration from the interactions of charged pions. When the energy of a particle falls below the threshold for multiple pion production, $\approx$ 1 GeV, the dominant energy loss becomes ionization. The importance of the hadronic core is that it feeds the electromagnetic and muonic channels through the production of neutral and charged pions as it penetrates deeper into the atmosphere.

The dominant shower component, in terms of numbers of particles, is electromagnetic. An EAS initiated by a $10^{18}$ eV cosmic ray will have in the neighborhood of $10^9$ electrons and positrons in the electromagnetic channel at the shower maximum. This shower constituent results from electromagnetic cascades [57] initiated by photons from neutral pion decays. The neutral pions are primarily the products of interactions between the hadronic core of the shower with the surrounding medium. Once these primary photons have initiated the electromagnetic cascade, the dominant processes are pair production by the photons and bremsstrahlung by the electrons and positrons. The electromagnetic component characteristically grows and then decays quickly as the consituent electrons and positrons drop below a critical energy of around 80 MeV. Below this energy the electrons quickly lose their remaining energy to ionization. Because the bulk of the shower energy ends up in the electromagnetic channel, most of the energy of the shower is eventually dumped into the atmosphere via ionization.

The final component of the shower is muonic. This portion of the shower results from the decay of charged pions and kaons. The behavior of the muonic component is distinct from the others in that, due to the stability of the muon and its low cross section, the number of muons grows to a maximum but then decays away very slowly. Because muons with energy below 1 GeV are only mildly relativistic and decay in physically short distances, the higher energy mouns are of greater interest. The number of muons with energy above this threshold is roughly $10^8$,

which is only an order of magnitude less than the number of electrons. Due to the suppression of muon bremsstrahlung by a factor $(m_e/m_\mu)^2 \sim 2.5 \cdot 10^{-5}$, the muonic channel does not produce an electromagnetic cascade and very little of the energy of this channel is deposited in the atmosphere. Charged pions and kaons are products of the hadronic core and are not expected to be present in an EAS initiated by an EHE photon. For this reason, many experiments search for PeV $\gamma$-ray initiated events by looking for events with a minimal muon content.

The signal detected by the FE experiment is due to the electromagnetic component of the EAS. The interaction of the electrons in the shower with the atmospheric nitrogen [19] causes the nitrogen to fluoresce emitting 300 nm to 450 nm photons isotropically. The photon yield for this process is 4-5 photons/electron-meter. Due to a fortuitous cancellation of the pressure dependence of excitation rate and the pressure dependence of the flourescence efficiency through collisional de-excitation, the flourescent yield is nearly independent of altitude. This simplifies the analysis and makes the determination of shower parameters much less sensitive to reconstruction errors.

The characteristics of EAS in the EHE regime are dependent on the nature of the initiating cosmic ray. In the case of cosmic ray protons, the inelastic cross section, $\sigma^{inel}_{p-air}$, is measured to be 530 mb [5]. This corresponds to a 45 g/cm$^2$ interaction length in air. Under these conditions, the proton interacts in the atmosphere within the first few hundred g/cm$^2$ and develops to its maximum size roughly 800 g/cm$^2$ after the first interaction. The EAS electromagnetic channel then decays away and at a point some 2400 g/cm$^2$ past the initial interaction the EAS is taken to be reduced to the point where it can no longer be detected. In the case of photon initiated showers, the development is the same except for the lack of the muonic channel. The depth of peak shower development in the Hillas parameterization of photon showers [57] is 50 g/cm$^2$ deeper than that for a proton of comparable energy.

EAS initiated by heavy nuclei are treated, to first order, as the superposition of an appropriate number of nucleons. Iron nuclei with energy $5{\cdot}10^{18}$ eV can be roughly treated as the superposition of 56 proton showers with energy $8{\cdot}10^{16}$ eV. Because the depth of maximum for proton showers decreases 70 g/cm$^2$ [25] per decade decrease in energy, the subshowers will have mean maxima 80 g/cm$^2$ less deep than a $5 \cdot 10^{18}$ eV proton shower. This effect, known as the shower elongation rate, suggests that the depth of maximum of an iron initiated EAS will be around 80 g/cm$^2$ shallower than a proton initiated shower of the same energy. More careful modeling of iron showers predicts that such showers will develop faster and will reach shower maximum at around 700 g/cm$^2$ past the point of first interaction [47]. In addition to being shallower than proton initiated showers by 100 g/cm$^2$, these showers are also expected to show less fluctuation in the depth of shower maxima. If some particle, with a relatively small cross section, in the hadronic core of the EAS were to carry a significant fraction of the energy of the primary particle then such a shower would be expected to develop anomolously deep. The possibility of observing such deeply developing EAS is one of the motivations for this dissertation.

An important feature of EAS at these energies is the Čerenkov light generated by the ultra-relativistic particles of which it is composed. The Čerenkov light is a broad spectrum component of the light generated by the shower. Its contribution to the detection process is very geometry dependent. For most purposes, the Čerenkov light is seen as an obscuring contaminant which masks the signal from the electromagnetic channel of the shower. In other experimental contexts, however, it is a very useful EAS characteristic from which the total energy of the shower can be reconstructed.

## 2.2 The Fly's Eye Detector

The experiment consists of two optical detectors, Fly's Eye I (FEI) and Fly's Eye II (FEII) at altitudes of 1.594 km (860 g/cm$^2$) and 1.457 km (875 g/cm$^2$) respectively. The sites are located in the western Utah desert at the Dugway Proving Ground. FEI consists of 67 1.6 m diameter front surface mirrors each with 12 or 14 photomultiplier tubes (PMTs)(90 mm diameter) at the focal plane. Each of the 880 PMT's, together with its Winston cone, has a 5.5° field of view resulting in full $2\pi$ steradian coverage of the night sky. At a distance of 3.4 km FEII is a similiar system consisting of 36 mirrors that view the portion of the night sky in the direction of FEI. The detectors are operated on clear moonless nights for a duty cycle of ~10%. FEI has been in operation since November 1981 and FEII since November 1985.

This detector was designed to indirectly detect the Extensive Air Shower (EAS) that results from the interaction of a cosmic ray with the atmosphere. These EAS are detected via the nitrogen flourescence they induce during their development within, and transit through, the atmosphere. In spite of the low efficiency of the flourescence (or scintillation) process, roughly 0.5%m, the large number of particles in an EAS produced by a cosmic ray with energy $\geq 10^{17}$eV makes this technique feasible for EHE cosmic rays. The isotropic nature of the flourescence light allows detection of EAS with a wide range of geometries. The principal limitation on the geometry of detectable events is that they not be more than about 40 km from the detector due to atmospheric extinction. Under some circumstances portions of EHE EAS can be detected as far as 60 km from the eye. Events that are propagating directly towards the detector are not normally detectable.

The actual data are collected through a sample and hold process that stores the integrated current from PMTs that view the EAS as well as the PMT trigger time. As a result, the FE detector tracks the development of the EAS as it passes through

the atmosphere. This ability to directly monitor the longitudinal characteristics of an EAS is unique to the FE experiment.

Given the known geometry of the detector and the PMT data the geometry of the EAS can, in principal, be reconstructed. Due to interplay between data uncertainties and the reconstruction process, certain EAS geometries are not reconstructable. In addition, other EAS geometries result in contamination of the data with Čerenkov light from the ultra-relativistic particles in the shower. For EAS whose geometry is reconstructable it is then possible to calculate the number of particles, primarily electrons, in the shower as a function of depth in the atmosphere. This yields what is called the shower profile. A fit of a model of shower development to the shower profile yields E, the shower energy, $N_{max}$, the peak number of particles in the shower, and $X_{max}$, the depth at which shower development peaks. These are the essential parameters used to characterize the cosmic rays.

### 2.2.1 Reconstruction of Shower Geometry

The reconstruction of the geometry of a given EAS is accomplished in one of two ways depending on whether the shower was seen by just FEI or by FEI and FEII simultaneously. Showers seen by a single detector must be reconstructed by a 'monocular' technique while showers seen by both detectors may be reconstructed by a 'stereo' technique as well. Stereo reconstruction is preferred because it results in substantially better reconstruction of the EAS geometry. The trade off is that the data rate for stereo events is much lower than for monocular events. Because the events sought in this dissertation are so rare the monocular data base was used to provide the best possible chance of observing such events. As a result, a careful consideration of monocular reconstruction errors was needed. This section is intended to describe the reconstruction process and indicate the sources of error.

Stereo reconstruction of the EAS (or track) geometry is quite simple from both a conceptual and calculational perspective. At a given detector the PMTs that trigger define a plane in the atmosphere that contains the EAS. Because the pointing direction of each PMT is known then the vector normal to the plane of the shower can be easily generated from the pointing vectors of the PMTs that view the shower. More precisely a weighted cross product of all the triggered tubes is used to define the normal vector to the plane of the shower. The errors in this part of the reconstruction are small, typically between 1° and 2°. The uncertainty in determining the shower plane is dominated by the 5.5° field of view of the PMTs. Once the shower plane from each detector is calculated it is straightforward to find the intersection of the two planes thereby defining the trajectory of the EAS. Except in cases where the two shower planes are nearly parallel this process yields a very accurate determination of the shower geometry.

For monocular reconstruction the PMT trigger times are needed in addition to the pointing directions. It is simply shown [8] that the dependence of the arrival time of light on the particualr portion of the EAS view by the i'th triggered PMT is given by the following expression.

$$\chi_i(t_i) = \chi_0 - 2 \cdot tan^{-1}\left[c(t_i - t_0)/R_p\right] \tag{2.1}$$

The best fit of the observed data to this function yields the parameters $\chi_0$ and $R_p$ which, along with the plane normal, completely define the shower geometry (Figure 2.1). Accurate reconstruction results when observed track lengths are longer than 50°. For shorter track lengths, $R_p$ and the plane normal, $\theta_n$, continue to be well reconstructed but the determination of $\chi_0$ is degraded. This is primarily the result of the low curvature of the arctangent function for small angles coupled with the noise in the timing measurement.

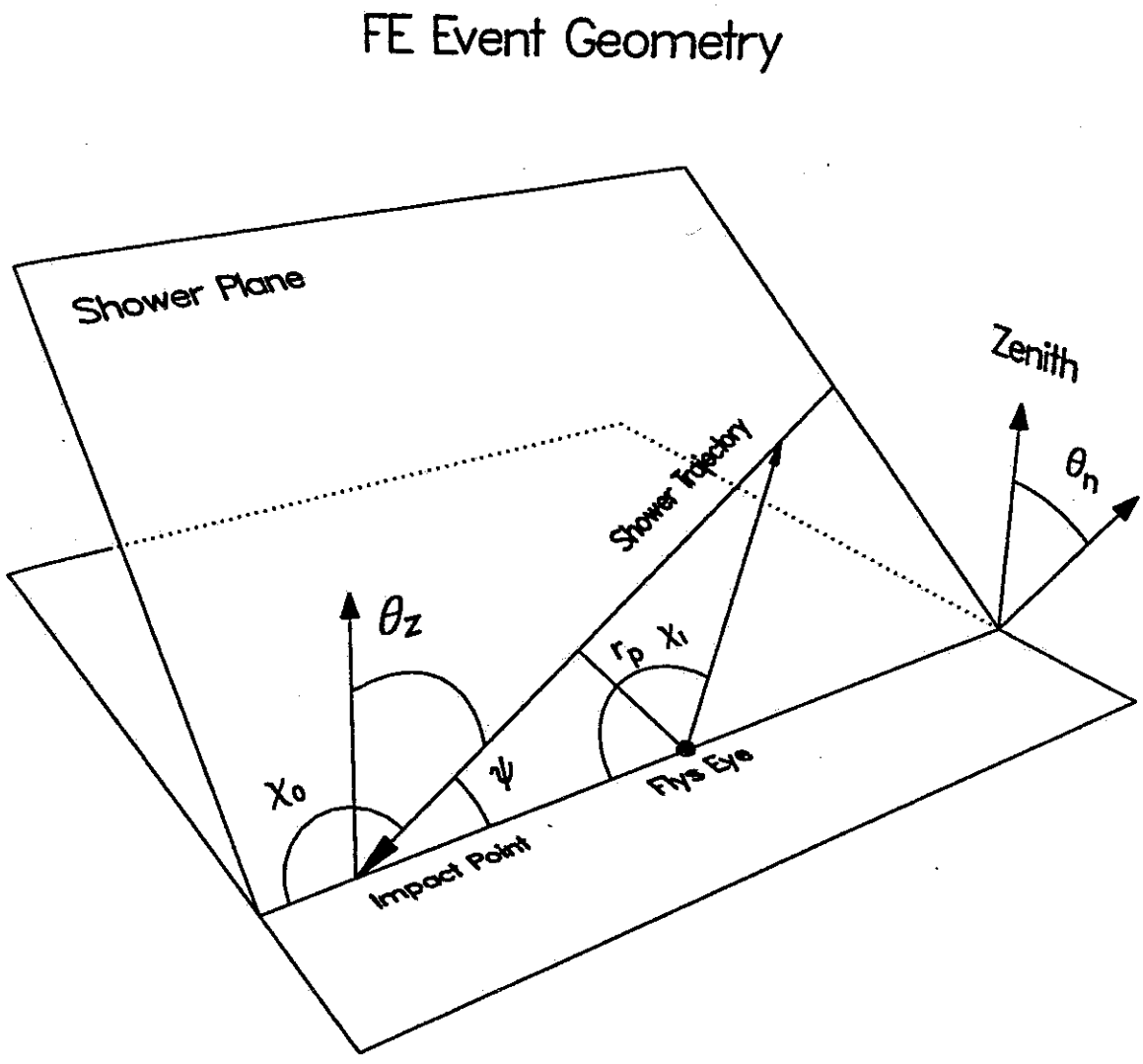


Figure 2.1. Geometry of EAS at FE with principal shower parameters labelled.

## 2.3 Detector Aperture

Equation 2.2 gives the number of events expected between energy $E_1$ and $E_2$.

$$N(E_1, E_2) = \tau \int_{E_1}^{E_2} \Omega(E) \frac{dN(E)}{dE} dE \tag{2.2}$$

where

$N(E_1, E_2)$ $\Leftrightarrow$ expected events between $E_1$ and $E_2$
$\tau$ $\Leftrightarrow$ detector on time (s)
$\Omega(E)$ $\Leftrightarrow$ detector aperture ($cm^2$-sr)
$dN(E)/dE$ $\Leftrightarrow$ differential particle flux ($(cm^2\text{-s-sr-GeV})^{-1}$)

$\Omega(E)$ includes geometric factor and the triggering efficiency of the detector for some class of potentially detectable events. The geometric factor is straightforward and consists of the solid angle acceptance of the Fly's Eye, which is effectively $2\pi$, and the effective area of the detector. The area factor is given by $\pi(r_p^{max})^2$. In addition $\Omega(E)$ also includes the triggering efficiency for the class of events being considered. This is the primary source of the energy dependence of the detector aperture. The Fly's Eye detector has a lower energy threshold due to the combined effects of photon collection optics and PMT gain at around $1 \cdot 10^{17}$ eV. The detector aperture increases two orders of magnitude at $10^{18}$ eV and continues to rise slowly until it flattens out near $3 \cdot 10^{19}$ eV.

The detector aperture can be calculated in at least two ways. The first is to measure the response of the detector to a fully characterized flux of particles. This method is especially effective if the particles used to characterize the detector are closely related to those being studied. There is no possibility of applying this method to the FE. The alternative, and that used by the FE experiment, is to develop a sophisticated computer model of the detector. This detector simulator must emulate ever nuance of the performance of the detector as accurately as possible. In the case of the Fly's Eye detector this includes the atmosphere, mirror optics, PMT cathode efficiencies, as well as the triggering and data collecting

electronics. Then, using Monte Carlo techniques, the response of the detector to various assumed particle fluxes can be calculated. As is the case for all such detector Monte Carlo programs the aperture calculation is only as good as the modeling of the system.

### 2.3.1 Detector Simulation

The detector simulation program has been previously described [8, 50] although many of the details are not given. What follows is a simplified representation of the flow of data through the simulation. The process begins by generating the geometric parameters of the shower from the appropriate probability distributions. Other interaction parameters such as inelasticity or particle energy are also generated at this point as needed. From the shower geometry the PMTs that view the shower trajectory are identified. Next, the time at which the light from the EAS arrives at each PMT that views the track is calculated. This is followed by a careful calculation of the amount of light reaching the PMT. The calculation includes the fluorescent yield, Čerenkov light production, scattering of both scintillation and Čerenkov photons between the track and the detector from Rayleigh and Mie scattering, mirror reflectivities, and Winston cone reflectivity. This light pulse is then passed to the electronics simulation routine, which yields the predicted signal levels as well as identifying the PMTs that triggered. Throughout this process statistical fluctuations of detector response functions based on empirical measurements are included. Finally the list of triggered PMTs and trigger times are checked to see that they satisfy the coincidence requirements for a detectable event. Events that satisfy all the detector requirements are written to a data file that emulates the raw data file written by the detector. The events in this simulation file are then analyzed in a manner identical to the 'real' data.

For the purposes of this dissertation the detector Monte Carlo is assumed to accurately reflect the behavior of the FE detector. Whether this assumption is justified will be tested and discussed at appropriate points later in this dissertation.

particles of interest in this dissertation are the leptons. In the following sections the plausibility of each of the leptons as a source of deeply penetrating showers will be examined.

### 3.1.1 Neutrinos

Neutrinos ($\nu$'s) will characteristically interact deep in the atmosphere. If the neutrino flux is large enough that there is a significant probability of an EAS being initiated within the fiducial volume of the Fly's Eye then $\nu$'s must be considered as a plausible source of deeply penetrating events. The sources of neutrinos in the EHE cosmic ray flux can be divided into astrophysical, those that originate outside the earth's atmosphere, and secondary, those that are the byproduct of other cosmic ray interactions with the atmosphere.

Astrophysical neutrinos with EHE energies are produced in a variety of ways. One source is the interaction of extragalactic cosmic ray nuclei with the 2.7° microwave background which yields secondary neutrinos through a number of channels [87]. The number of such neutrinos is dependent on the assumed flux of sufficiently energetic cosmic ray nuclei and the photon environment through which they propagate. The stability of the neutrino combined with its low cross section means that its effective lifetime is easily comparable to the age of the universe. As a result, sources of neutrinos from much earlier stages in the evolution of the universe need to be considered. This also means that evolutionary effects in the universe must be taken into account when considering such sources. Due to the diffuse nature of this source the astrophysical neutrino flux should be isotropic. In Chapter 6 a specific prediction, from Hill and Schramm [58], of the EHE neutrino flux due to this mechanism will be discussed in detail. To get a rough feel for the plausibility of this mechanism consider the $\nu$ flux predicted by Hill and Schramm. At $3 \cdot 10^{17}$ eV the differential flux of astrophysical neutrinos could be a large as

$10^{-22}$ (cm$^2$-s-sr-GeV)$^{-1}$. Taking a reasonable estimate for the fiducial volume of the FE, this leads to the expectation that $6 \cdot 10^7$ neutrinos of this energy have passed through the FE detector volume during its operation. Taking a pathlength through the detector of $10^4$ g/cm$^2$ indicates that roughly 100 of these neutrinos would interact inside the detector volume. If the triggering efficiency is on the order of a few percent there should be several neutrino initiated events in the data set.

EHE neutrinos are also expected to be produced in large numbers by Active Galactic Nuclei (AGN's) and other compact objects [88]. The neutrino flux calculated for these sources is subject to many uncertainties. For certain scenarios it has been suggested that this mechanism would lead to neutrino fluxes comparable to those discussed in the context of the Hill and Schramm model. Although this mechanism is intrinsically a point source of neutrinos an isotropic flux is expected when an integration over all such sources is performed. It is important to note that if such a source occurs within the local supercluster, then some anisotropy in the neutrino flux would be predicted [88].

The flux of neutrinos due to interactions of cosmic rays with the atmosphere is significant. Many neutrinos are produced via the decay of charged mesons in the EAS. Volkova [91] has calculated the integrated atmospheric neutrino flux due to both direct and secondary processes. Volkova finds that at energies above $10^{15}$ eV direct processes dominate the integral spectrum. The resulting integral spectrum shows an $E^{-2}$ dependence and when extrapolated to $10^{18}$ eV leads to a predicted differential neutrino flux of $10^{-26}$ (cm$^2$-s-sr-GeV)$^{-1}$. This flux, which is already well below that of the previously described astrophysical sources, must be further reduced by a factor of $10^{-4}$. This is because the FE experiment is only sensitive to electron neutrinos which Volkova states constitute 1 part in $10^4$ of the total flux at these energies. For these reasons atmospheric neutrinos will not be considered as a

potential source of detectable deeply penetrating EAS.

A measurement of the neutrino flux at EHE energies would ideally include a neutrino spectrum, that is to say flux as a function of energy, as well as a measurement of neutrino anisotropy. Given such a measurement, the models of both source scenarios given above could likely be constrained. However, considering the previously estimated size of the neutrino data set the statistics for such a clear measurement at EHE energies are unlikely to be obtained by any experiment in the forseeable future. In the more likely event that only a handful, if any, such neutrino events are detected, then only very crude constraints can be placed on the source models. Fortunately, even such crude constraints would provide information useful to astrophysics. As will be seen in Capter 6, such constraints could set upper limits on the maximum redshift of sources contributing to the neutrino flux or limits on some parameters of AGN models.

### 3.1.2 Charged Leptons

The charged leptons need to be considered separately in the context of deeply penetrating showers. Electrons, which are not part of the primary cosmic ray flux, generate detectable EAS. An electron initiates a standard electromagnetic shower through ionization losses, bremsstrahlung, and to a lesser extent other discrete loss mechanisms. The dominant loss process in electron propagation is bremsstrahlung which has a characteristic length scale of $\sim 37$ g/cm$^2$ in air. As a result, such EAS are substantially similiar to showers initiated by protons which have a mean interaction length of 45 g/cm$^2$. Because of this, electrons will not contribute to the flux of deeply penetrating events.

The case for muon initiated deeply penetrating EAS needs to be addressed with more care. As discussed in the context of EAS development muons are a major secondary component of the shower. With a lifetime of $\sim 2 \cdot 10^{-6}$ s an EHE muon

propagates great distances ($\sim 10^9$ km) in the absence of significant energy loss mechanisms. In fact, the decay of an EHE muon produced in an atmospheric EAS will not take place above ground except for the most extreme geometries. This means that secondary EHE muons will not produce EAS within the fiducial volume of the FE due to decay processes. The remaining possibility for detection of muons is through the muonic equivalent of the electromagnetic shower generated by an electron. The determining difference in the case of muons is that [46, pp76] bremsstrahlung is no longer the dominant loss mechanism due to supression by a $(m_e/m_\mu)^2$ factor. As a result, the energy loss by the muon as it transits the atmosphere is too low to be detectable by the FE even at EHE energies. A final consideration is the flux of muons with energies above the FE detection threshold. An estimate of the EHE atmospheric muon flux yields a flux of $10^{-40}$ (cm$^2$-s-sr-GeV)$^{-1}$ [46, pp207] which is far too small to be detectable.

The effects described indicate that muons produced in EHE EAS do not contribute significantly to the flux of deeply penetrating particles in the FE data set. Secondary muons from interactions of the cosmic ray flux with the interstellar medium are also a negligible source of deeply penetrating showers. In spite of the long lifetime and attendent propagation length in an atmospheric sense the EHE muon propagation length is essentially zero on astrophysical scales. This means the constant muonic component of the cosmic ray flux can be taken to be zero.

The tau ($\tau$) is a more reasonable source of deeply penetrating showers than the muon. The $\tau$ has a much shorter lifetime, $\sim 3 \cdot 10^{-13}$ s, than the $\mu$, leading to decay before ground impact for many plausible geometries. The tau shares the muon's low energy loss rate resulting in no detectable energy being deposited along its trajectory. Thus, essentially no primary energy is lost before the $\tau$ decays deep in the atmosphere. As a consequence the production of tau is the deciding factor in evaluating the potential contribution to the flux of deeply penetrating particles. The

primary source of tau as a secondary particle in EAS is from the decay of bottom and top quarks. Charmed hardrons are almost all too light to decay via tau production. As will be seen in the following section the production of bottom is expected to be strongly suppressed relative to charm. The principal decay modes for B mesons are through K and $\pi$ production. The $\Upsilon$ meson decays with roughly equal probability through tau, muon, and electron channels. Because of their lighter mass, $\sim$ 5.2 GeV/$c^2$, compared to the $\Upsilon$, $\sim$ 9.4 GeV/$c^2$, the production of B mesons will be somewhat favored resulting in further suppresion of this $\tau$ production process. All of this taken together implies that while the tau is a reasonable candidate to initiate a deeply penetrating event the production rate is so low relative to other potential sources that there is little or no contribution to the flux of deeply penetrating particles. Because, as will be seen in the next section, the production of top qaurks is expected to be suppressed by at least an order of magnitude relative to bottom quarks, it is not expected to contribute a significant $\tau$ flux.

In summary, consideration of the properties of the charged leptons indicates that they are not expected to contribute in any significant way to the flux of deeply penetrating events. Any measurement of the flux of deeply penetrating particles will have little to say about the physics of charged leptons.

## 3.2 Heavy Quarks

The production of hadrons containing 'heavy' quarks provides another possible source of deeply penetrating showers under certain conditions. In this context, 'heavy' is taken to mean charm, bottom, and top quarks. If, in the initial interaction(s) of the primary cosmic ray particle, a hadron containing heavy quarks is produced then there may be a reasonable probability that such a hadron carries away a substantial fraction of the energy of the primary. Such an effect will depend on the Feynman $x_F$ distribution of the heavy quark matter produced. The Feynman

$x_F$ parameter is the ratio of the energy of the secondary particle to that of the primary. Given the conservation of flavor in strong and electromagnetic interactions this heavy hadron will propagate as a heavy hadron until it decays via the weak interaction. As the heavy hadron propagates it will lose energy, primarily through inelastic collisions. Significant loss of energy during propagation will reduce the energy available for deposition deep in the atmosphere. For a particular set of particle characteristics it is possible that such a heavy hadron could propagate deep into the atmosphere with minimal loss of energy and then decay producing a deeply penetrating shower. It is apparent that there are a number of conditions that must be met in order for this process to be plausible. These conditions are summarized in the following list.

1 - suitable production rate for heavy hadrons

2 - sufficient energy in heavy hadron produced

3 - appropriate lifetime to yield deep decay

4 - minimal energy loss during propagation

5 - suitable decay products to initiate EAS

As an example, assume that a primary cosmic ray proton that produces the heavy hadron has an energy of $3 \cdot 10^{18}$ eV and is proceeding along a trajectory that impacts the earth at a depth of around 2500 g/cm$^2$. Because the proton interacts in the first few hundred grams the heavy hadron must traverse approximately 1000 g/cm$^2$ to decay deep in the atmosphere. A shower that begins at a depth of 1200 g/cm$^2$ is a deep shower based on the existing data from the FE experiment.

Conditions 1) and 2) require that a heavy hadron is produced with an energy greater than, or comparable to, the threshold energy of the Fly's Eye detector of $10^{17}$ eV. In order for this to be the case the heavy hadron must carry a significant

fraction of the energy of the EHE cosmic ray primary. This corresponds to a significant differential cross section for hard $x_F$ production of the heavy hadron. For the FE detector to have a significant probability of detecting such an event, there must be roughly 100 cosmic ray interaction that produce an energetic heavy hadron in the fiducial volume of the detector. Taking the cosmic ray spectrum as calculated by the FE experiment [8] and integrating over energies greater than 1 EeV, approximately $10^5$ normal cosmic ray initiated EAS are expected. The net effect is that the required cross section for the production of large $x_F$ heavy hadrons is $\approx 10^{-3} \cdot \sigma_{p-air}$.

A deep trajectory passing through the Fly's Eye detector volume would travel approximately 30 km through the atmosphere and traverse 1000 g/cm$^2$. Given a heavy hadron mass of around 3 GeV/c$^2$ the lifetime of a particle that can traverse such a distance before decaying is bounded from below by the following;

$$\tau_q \geq l/(c \cdot \gamma) \tag{3.1}$$

where

| | | |
|---|---|---|
| l | $\Leftrightarrow$ | distance along trajectory |
| c | $\Leftrightarrow$ | speed of light |
| $\gamma$ | $\Leftrightarrow$ | relativistic $\gamma$ of heavy hadron |

For the given trajectory and assumed heavy hadron mass this expression leads to $\tau_{hh} \geq 1 \cdot 10^{-13}$ s.

To satisfy condition 4), the 1000 g/cm$^2$ must be traversed with a minimal loss of energy which is taken to mean an energy loss no greater than 90%. Energy loss depends both on the interaction length and the elasticity of such interactions when they occur. The energy loss constraint requires that either the interaction length is long, i.e., $\geq$ 300g/cm$^2$, with an average inelasticity of .5 or the interaction

length is more modest, $\geq$ 100 g/cm$^2$, with a lower average inelasticity around .1. In either case the underlying constraint is that the decay of the heavy hadron will be undetectable if its energy, at decay, is less than .1 EeV.

The final condition is satisfied if the heavy hadron decays primarily through pion, kaon, electron, and photon producing channels. Decay channels that yield muons and tau particles will not lead to detectable EAS due to the limited amount of energy deposited in the atmosphere by these particles.

The following list summarizes the quantitative portions of the general constraints.

1 - $10^{-3}$ heavy hadron production efficiency

2 - $\tau_{hh} \geq 1 \cdot 10^{-13}$ s

3 - either long interaction length , $\geq$ 300 g/cm$^2$ or low inelasticity, $\sim$ .1, or both

In examining the literature it is found that these constraints severely restrict the possible source of deeply penetrating showers from this type of source. The production of charmed hadrons at all $x_F$ is expected [9, 74] to be at the 1% level relative to the proton cross section while the production of bottom and top scales as $(m_q/m_c)^2$. This is primarily due to the intrinsic charm states in the structure of the nucleon [40]. In the same models, the Feynman x ($x_F$) distributions indicate that 10% to 20% of the total charm or bottom production has large $x_F$. In this context 'large' means $\geq$ 0.1. The result is a production efficiency for charm matter having large $x_F$ of $10^{-3}$. Bottom production will be suppressed by an order of magnitude and top production by at least 1000 assuming $m_t \geq 50$ GeV. This implies that charmed hadrons seem like plausible candidates for the production of deeply penetrating particles. Bottom production would contribute only marginally to this

process. Top production can be neglected in the context of deeply penetrating particles.

Many of the charm and bottom hadrons meet the lifetime requirement of $\tau_{hh} \geq 10^{-13}$ s. In the event that branching ratios for the production of charm and bottom at EHE energies were to be known or predicted, the lifetime constraint could be used to eliminate certain branches from consideration.

Finally, hadrons with heavy quark constituents may have somewhat reduced cross sections [72], leading to interaction lengths on the order of hundreds of g/cm$^2$. In the MIT bag model such a heavy quark component leads to increased localization of the hadron. This effect leads to a reduction in the cross section compared to a hadron with no heavy quark constituent There are also claims in the literature [63] that the mean inelasticity of heavy hadron-air interactions might be a low as .1. In the case of EAS initiated by protons there are models that predict larger mean inelasticities in proton-air interactions with increasing energy as well as models that predict significant decreases. Current Fly's Eye measurements are more consistent with models of increasing inelasticity.

In summary, charmed hadrons that carry a substantial fraction of an initial EHE cosmic ray interaction deep into the atmosphere must be considered as a source of deeply penetrating events. To a lesser extent hadrons with bottom may also contribute. Measurement of the flux of deeply penetrating showers due to this mechanism could provide data of interest to particle physics at energies higher than those available at any current or proposed terrestrial accelerator. The FE is sensitive to primary cosmic ray interactions with center of mass energy $\sqrt{s} \geq 15$ TeV while the Superconducting Super Collider (SSC), the highest energy terrestrial accelerator, is designed for $\sqrt{s} = 20$ TeV. There is an important difference between these instruments in that the Fly's Eye is primarily sensitive to the forward production region while the SSC is designed to investigate central production. In

spite of the fact that particle physics parameters are strongly coupled in the FE experiment the specific parameters addressed would include total heavy hadron production cross sections, $x_F$ distributions in heavy hadron production, heavy hadron interaction cross sections, and heavy hadron inelasticity distributions. The details of these effects and how they can be illuminated by the measurement of the deeply penetrating flux will be discuss in Chapter 7.

## 3.3 Exotic Matter

The 'Centauro' type events [16] found in the Mt. Chacaltaya emulsion exposures and reported by the Brasil-Japan collaboration have been singularly difficult to interpret. These events are characterized by their deeply penetrating nature, their large suggested rest mass, and their large multiplicity. The characteristics of these interactions effectively rule out almost all of the particles interactions that have been observed and studied to date. A number of proposals have been put forward to explain these events, all of which are all based on some sort of exotic state of matter. Among the possibilities are explosive quark globs [14], endopionic bags [29], and strangelets [93, 60]. There are no predictions of the fluxs of such unusual 'particles' in the EHE cosmic ray flux but they must be considered as possible source of deeply penetrating showers. Centauro type events should be readily distinguishable from events initiated by either charm or neutrinos due to the large observed multiplicity. This multiplicity would result in an EAS profile that develops much more quickly than a standard shower of the same energy.

# CHAPTER 4

# EVENT SIGNATURE

The fundamental empirical question of this dissertation is how to distinguish an event initiated by a deeply penetrating particle from those initiated by the nuclei which constitute the overwhelming bulk of events detected by the FE. This question can be asked in two different ways. What are the event characteristics that allow the positive identification of events that are due to deeply penetrating particles? What are the event characteristics that allow the positive identification of events that are not due to cosmic ray nuclei? Given that deeply penetrating events are intrinsically rare there is no empirical data base that allows us to identify the characteristics posited in the former version of the question. There is, however, a large data base of events that are due to cosmic ray nuclei. This means the question of what is, and by extension what is not, characteristic of events initiated by cosmic ray nuclei can be addressed with confidence. For this reason a signature of deeply penetrating events is sought such that they are not due to cosmic ray nuclei.

The principal EAS parameter that is associated with the shower depth is $X_{max}$. Showers that are initiated deep in the atmosphere will have shower maxima that are correspondingly deep. We define a deeply penetrating event as one whose $X_{max}$ is so deep in the atmosphere that the event is inconsistent, to some level of significance, with a standard cosmic ray shower. This chapter will discuss how a criterion is established to identify an event that is not initiated by an EHE cosmic ray nuclei and must therefore be a deeply penetrating event.

## 4.1 Qualitative Considerations

Because deeply penetrating events are expected to be rare, the first consideration is to analyze data from as early in the data pipeline as possible. In principle, this should lead to the largest possible data set in which to search for such rare events. The output of the geometric (GEO) analysis is the least processed data that still contains most of the pertinent event parameters. The GEO data have been subject to analysis designed to eliminate obvious noise events, laser shots, flashers, and airplanes from the data. There is also a minimal quality cut that requires five triggered tubes in an accepted event as well as some cuts on the timing of the tubes in the event. The important features of these data are that it has complete geometric information about the shower but has no estimates of either shower energy or profile. Choosing to work with the GEO data set means that the shower maximum, a feature of the shower profile, will not be accessible for event characterization. This is because further analysis by the SIZE and SHAPE routines is needed to reconstruct the shower profile from which $X_{max}$ is determined. Because a deep shower maximum is the feature that defines the events of interest to this dissertation the use of the GEO data set means an implicit constraint on $X_{max}$ must be sought.

Qualitatively, the matter traversed by an EAS to reach a particular point in the fiducial volume of the FE detector increases as the zenith angle ($\theta_z$) of the event increases. This means that, on average, detected EAS with large $\theta_z$ have larger $X_{max}$. For an individual event, however, large $\theta_z$ alone is not sufficient to support the conclusion that the event is deeply penetrating. The classic counter example is the horizontal shower ($\theta_z = 90°$) that is 15 km above the ground. Such an event can be shown to have an $X_{max}$ that is anything but deep. Large $\theta_z$ combined with nearness to the ground is required to yield the expectation that an event has

an unexpectedly deep $X_{max}$. The GEO data set contains sufficient information to design an event criterion of this kind.

An alternative approach is to note that the plane normal ($\theta_n$) provides a lower limit on $\theta_z$ (see Figure 2.1) while also providing some constraint on the proximity of the event to the earth.

In either case the fundamental question is what constitutes an unusually deep event in the desired parameter space? Figures 4.1 and 4.2 show typical distributions of the parameters in question. In both cases the range shown is the complete range of the parameter space. Note that in the case of $\theta z$ the full range is spanned by this small data set. In contrast, the $\theta_n$ distribution shows a significant region devoid of events. In order to identify events that fall outside the range of data resulting from typical cosmic rays it is important to be able to clearly define what the extent of that range is. It is not clear, in the case of the $\theta_z$ distribution, where that edge is. Conversely the $\theta_n$ distribution indicates a definite region where so called normal events are not expected. This suggests that $\theta_n$ may be the preferable parameter to use in characterizing deeply penetrating events.

An additional consideration is the accuracy with which $\theta_z$ and $\theta_n$ are determined in the analysis. Figures 4.3 and 4.4 show the distribution of the estimated errors in the determination of $\theta z$ and $\theta_n$. Even if the artifact at 90° in the $\theta_z$ error distribution is ignored, these distributions show dramatic differences. The mean uncertainty in the determination of $\theta_z$ is so large that a nearly horizontal event, a otherwise reasonable candidate deep event, could plausibly be either upward going or downward going with a very normal $X_{max}$. On the other hand, an event observed to be in a nearly horizontal plane is just that, given the mean $\theta_n$ error.

The reason for the difference in the error distributions is straightforward. $\theta_n$ is determined by which PMTs fired and the geometry of the FE detector. This geometry of the FE dectector has been carefully characterized and is subject to

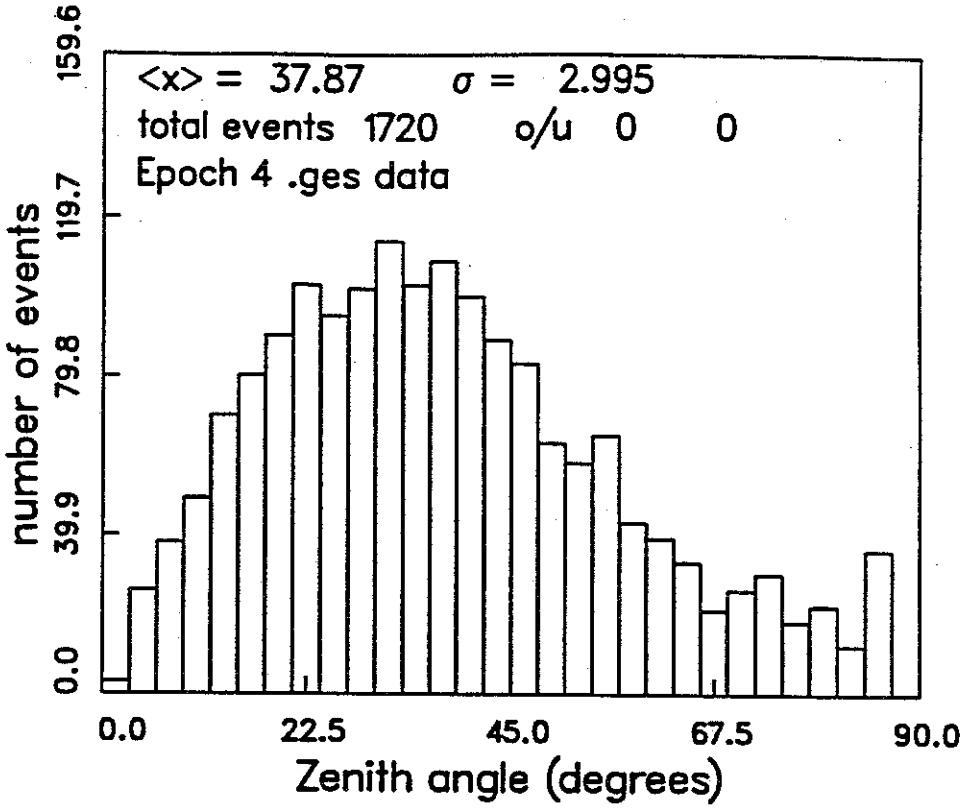


Figure 4.1. Distribution of $\theta_z$ from monocular events.

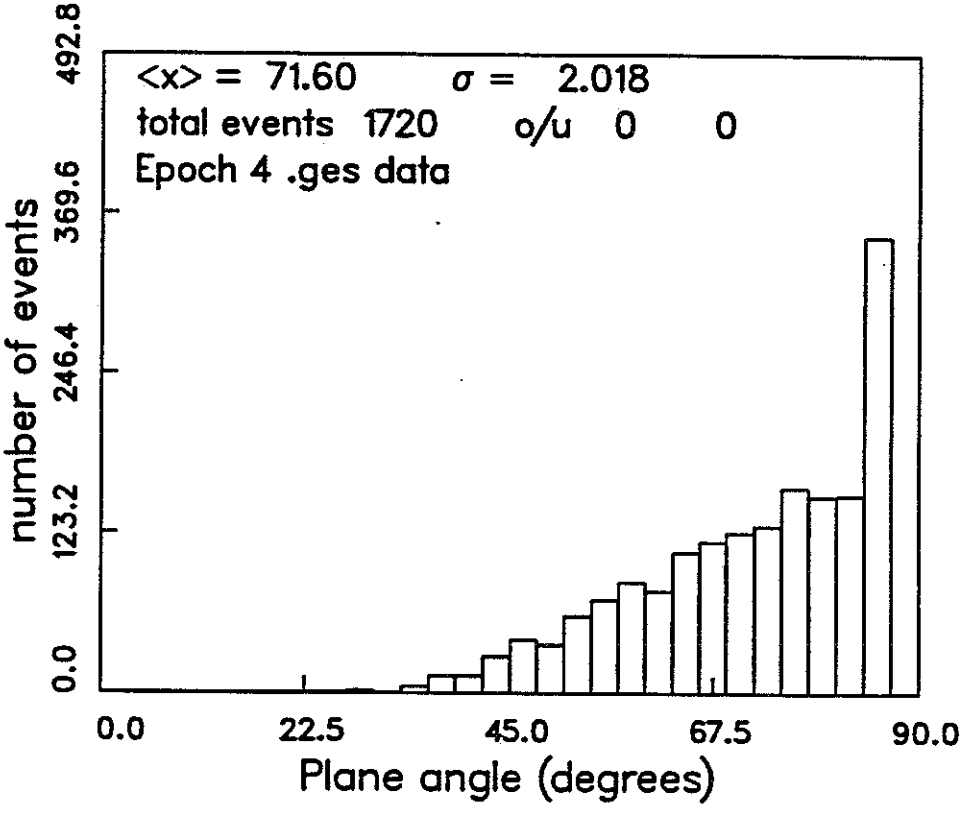


Figure 4.2. Distribution of $\theta_n$ from monocular events.

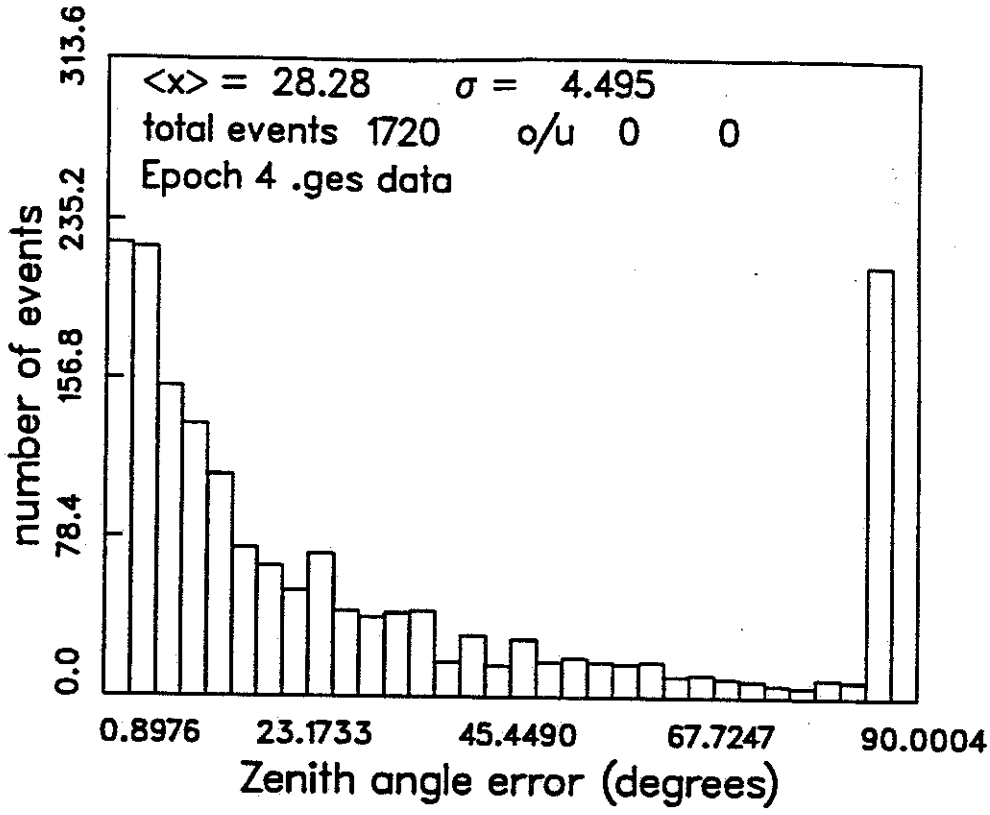


Figure 4.3. Error distribution for $\theta_z$ from monocular events.

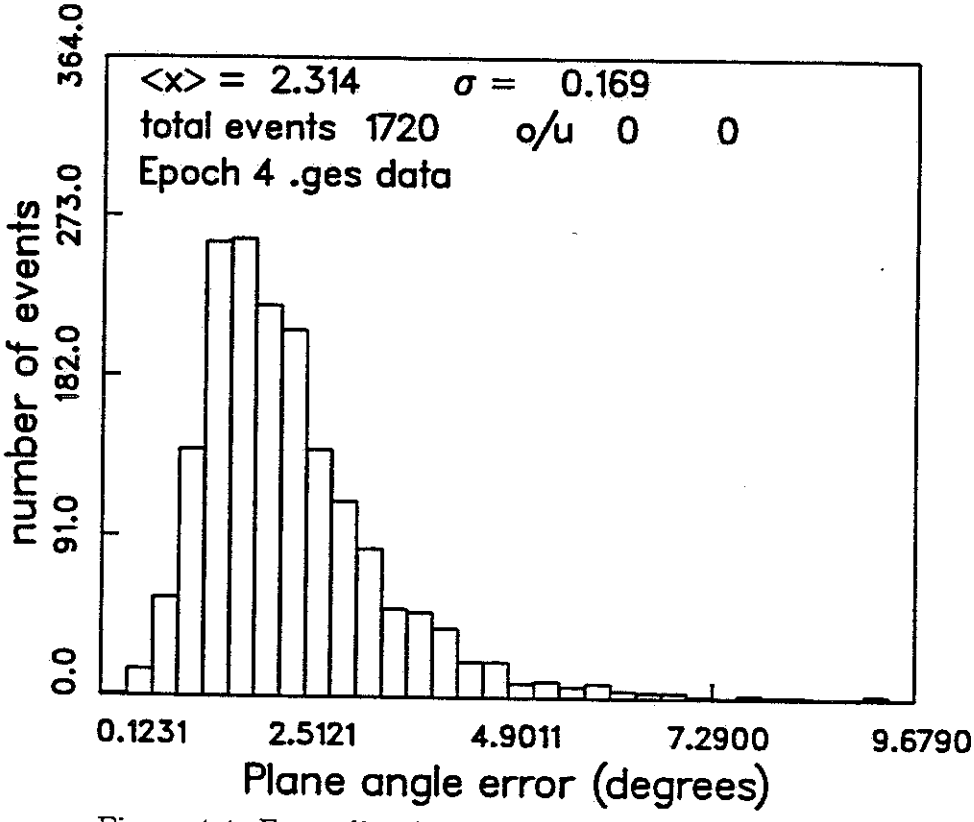


Figure 4.4. Error distribution for $\theta_n$ from monocular events.

a minimum of uncertainty. There is no uncertainty in knowing which tubes fired. The uncertainty in the determination of $\theta_n$ is primarily due to the 5.5° field of view of the PMT/Winston cone assembly combined with the track length. The determination of $\theta_z$ is additionally dependent on the timing information from the detector. Uncertainty in the firing time is due in part to characteristics of the detector electronics as well as jitter in the actual timing measurement. Due to the specific form of the fitting function the timing uncertainty leads to significant uncertainty in the fit particularily in the case of relatively short track lengths. The uncertainty in fit paramters in turn leads to substantial uncertainty in the determination of $\theta_z$.

The uncertainty in $\theta_z$ can be reduced by considering only events which have long track lengths. Typically events with track lengths greater than 50° will have a lower associated uncertainty. As can be seen in Figure 4.1, imposing such a track length requirement would reduce the data set by a factor of $\sim 2$. By requiring a 30° minimum track length the data set is not significantly reduced and the uncertainty in $\theta_n$ is acceptable. Because the minimum number of triggered PMTs in an event is set at 5, which roughly corresponds to a 25° track length, a 30° track length constraint also helps eliminate marginally triggered events.

For the purposes of this dissertation it was decided to implement an implicit constraint on the $X_{max}$ of a detected event through the plane normal angle, $\theta_n$. This approach will permit the consideration of relatively short track length events as potential deeply penetrating events while reducing the sensitivity of the search to uncertainty in the timing measurements.

### 4.1.1 Implementing $\theta_n$ Criterion

At this stage what needs to be determined is the distribution of events in $\theta_n$ space for normal cosmic ray events. This is accomplished through the event generator and

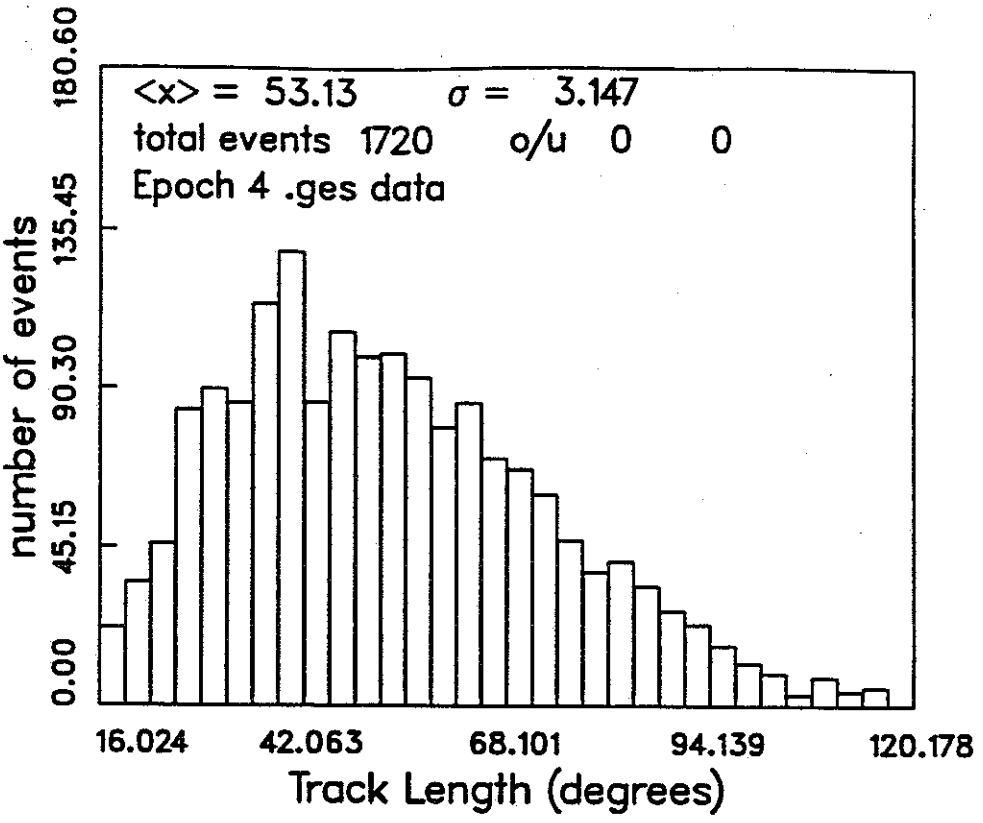


Figure 4.5. Track length distribution for typical monocular events.

detector simulator described in Chapter 2. Such an approach necessarily depends on the assumption that the monte carlo program accurately reflects the performance of the detector in all ways. The number of events generated and passed to the simulator is determined by the known operating time of the FE as well as the calculated and verified EHE cosmic ray spectrum. The $\theta_n$ distribution of the triggered events is then analyzed to define a suitable criterion for events that are not due to nominally normal cosmic rays.

In order to provide an acceptably reliable signature for deeply penetrating events the criterion will be based on the $\theta_n$ distribution of 100 times the number of cosmic ray events actually detected. This results in a confidence level of 99% that an event satisfying such a signature for deeply penetrating events will not be due to a normal cosmic ray. The $\theta_n$ distribution resulting from such a calculation is shown in Figure 4.6. An important feature of this plot is the abrupt discontinuity in

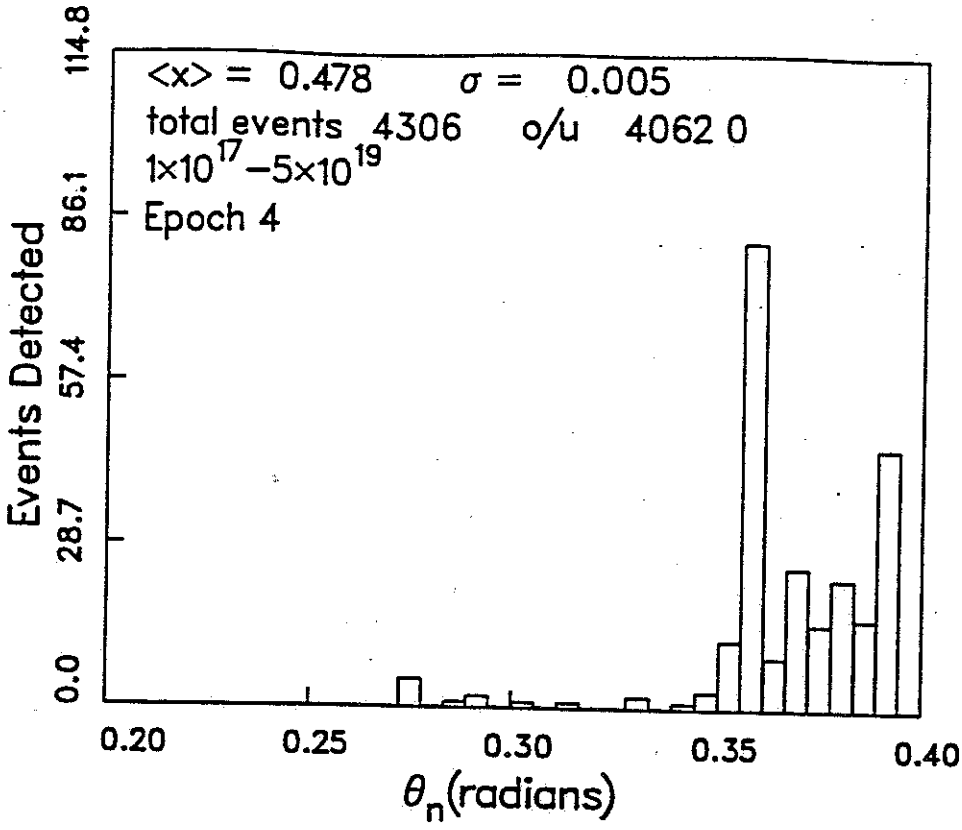


Figure 4.6. $\theta_n$ distribution of triggered events from Monte Carlo data. Events generated $\theta_z$ between 60° and 89°.

the tail of the distribution at 19.5 °. This discontinuity is a result of the 3-tube local coincidence requirement for ring 5 mirrors. Events that occur in planes with $\theta_n \leq 20°$ require at least one mirror in ring 5 to trigger in order to meet the master coincidence requirement of two triggered mirrors. EAS in planes with $\theta_n \leq 16°$ are viewed exclusively by ring 5 mirrors. This may be the dominant reason why the $\theta_n$ distribution cuts off between 15° and 16°. The implication of this distribution is that if the FE experiment were to amass an on-time 100 times that currently represented by the data set there would still be no standard hadronic events expected with $\theta_n \leq 15°$. As a result if an event exists in the current data set with a $\theta_n$ less than the cutoff value then such an event is not initiated by a standard cosmic ray and must be a deeply penetrating event. Table 4.1 gives the cutoff values for epochs 2 through 4.

Table 4.1. $\theta_n$ cutoff values in degrees for each epoch based on 100 times the actual number of detected FE events. Confidence Limits (C.L.) are given based on the analysis in the text.

| Epoch | 99% C.L. | 90% C.L. |
|---|---|---|
| Epoch 2 | 15° | 20° |
| Epoch 3 | 15° | 20° |
| Epoch 4 | 15° | 20° |

The confidence limits given reflect the probability that an event in the data set with $\theta_n$ less than the stated value is not due to a normal cosmic ray event. The confidence level is arrived at in the following manner. For $k$ events that triggered the detector simulator the probability that the actual mean number of events is $\mu$ is $P(\mu|k)$ which can be expressed using Bayes' Theorem as

$$P(\mu|k) = \frac{P(k|\mu)P(\mu)}{\int_0^\infty P(k|\mu)P(\mu)d\mu}. \tag{4.1}$$

In this expression, $P(k|\mu)$ is the probability that $k$ events are observed from a Poisson distribution with mean $\mu$. $P(\mu)$ is the probability that the mean is $\mu$ and is taken to be a uniform distribution. The expected value of $\mu$ is then given by

$$\bar{\mu} = \int_0^\infty \mu P(\mu|k)d\mu. \tag{4.2}$$

$\bar{\mu}$ is the expected mean number of events in the Monte Carlo data set which represents 100 times the actual data set. This leads to the expected mean number of hadronic events in the actual data set being $\bar{\mu}/100$. From this the probability that no hadronic events are found in the aperture of interest is given by

$$P(0|\bar{\mu}) = e^{-\bar{\mu}/100} = C.L. \tag{4.3}$$

This analysis suggests that deeply penetrating events are those with $\theta_n \leq 20°$. The effect of reconstruction errors on this signature will now be considered.

## 4.2 Spillover

Some deeply penetrating events with $\theta_n \leq 20°$ will be reconstructed with $\theta_n \geq 20°$ but an equal number with $\theta_n \geq 20°$ will reconstruct with $\theta_n \leq 20°$. The concern is that normal hadronic events may be reconstructed with a $\theta_n \leq 20°$. To address this question the following check was performed. A large number of events were randomly generated with some fixed $\theta_n$. These events were then passed to a detector simulator program [8], which generates a simulated data file. This data file is then analyzed using the normal data analysis routines and the $\theta_n$ of the reconstructed showers are compared to the actual or generated values. The result of this exercise is that the distribution of $\theta_n$ for the reconstructed showers had the same mean value as the distribution for the generated showers with a standard deviation of $\sim .6°$. This test was performed for $17° \leq \theta_n \leq 20°$. Choosing the $\theta_n$ criterion to be $3\sigma$ less than the nominal value given previously would result in a mimimal chance that a normal event is erroneously reconstructed and meets the requirement for a deep event. For this reason the criterion for deeply penetrating events is modified to be: *Candidate deeply penetrating events are those whose $\theta_n$ is less than 18°.*

## 4.3 Upward Going Events

Upward going events provide the classic signature for EAS initiated by neutrinos. There is no question that an event that is demonstrably upward going, except for some limited geometries, is a deeply penetrating event. Such an event would either have to traverse an enormous amount of atmosphere or some portion of earth as well as the atmosphere. These events would be deeply penetrating in the extreme. For most geometries the amount of matter traversed by such a shower would be opaque to all charged leptons leading to the identification of upward going events as neutrino initiated EAS. Upward going events are identified by shower zenith angles

greater than 90°. Because $\theta_z$ is subject to different uncertainties than $\theta_n$ a different criterion for candidate upward going events must be selected.

### 4.3.1 Zenith Angle Resolution

For an event to be convincingly upward going, it must have a zenith angle greater than 90° with estimated reconstruction errors small enough that the event is clearly not downward going. As can be seen from the earlier discussion of the error distribution of $\theta_z$, an event would be unlikely to be convincingly upward going unless $\theta_z$ were greater than 100°. Considering only events with track lengths $\geq 50°$ reduces the mean uncertainty in the determination of $\theta_z$ to roughly 2° along with a reduction is the size of the data set. Nearly horizontal events would have to be considered to be downward going and subjected to the previously defined $\theta_n$ criterion. This leads to the definition of the signature of an upward going deeply penetrating event as one whose $\theta_z \geq 100°$ with a track length greater than 50°. Apparently upward going events with $\theta_z \leq 100°$ must meet the same requirement as downward going events.

### 4.3.2 Neutrino Flux Attenuation

Due to the shadowing of the earth, there is a substantial energy-dependent attenuation of deeply penetrating events with $\theta_z \geq 90°$. Figure 4.7 shows the calculated attenuation of neutrino events as a function of zenith angle based on the EHE neutrino interaction cross sections of Quigg *et al.*[82]. As can be seen, the minimum attenuation of the neutrino flux at $\theta_z \geq 100°$ is $10^1$ at $10^{17}$eV and is substantially larger at higher energies. Assuming that the triggering efficiency for upward going events is the same as that for downward going events, an estimate of the aperture for upward going neutrino events can be made. Relative to the

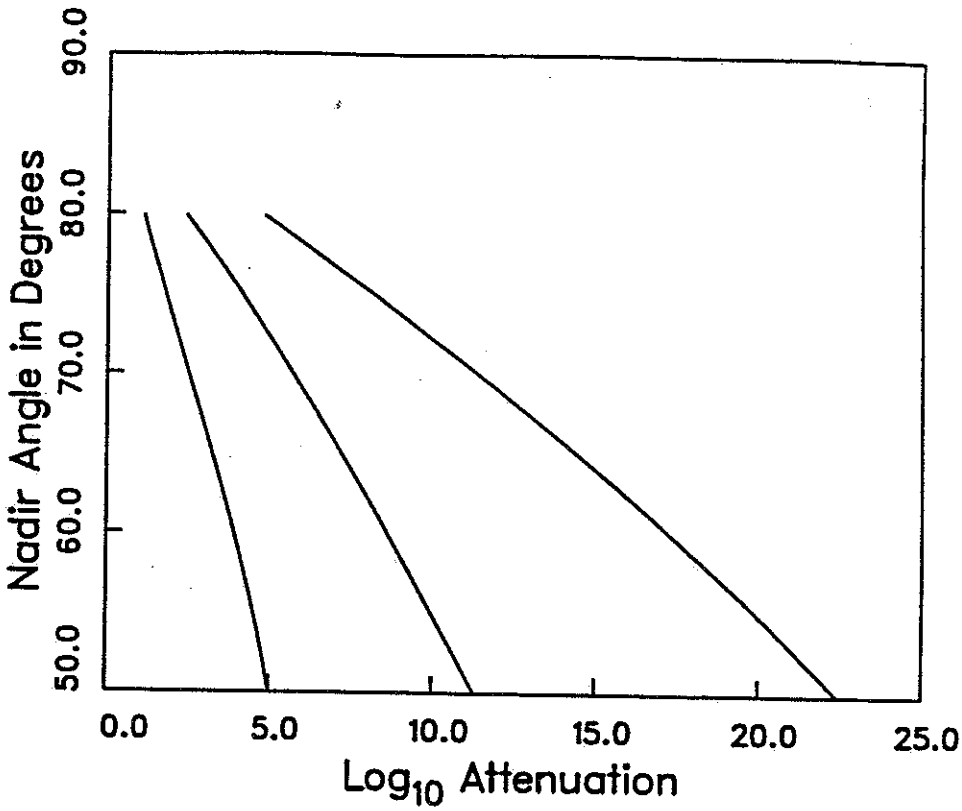


Figure 4.7. Attenuation of neutrino flux due to passage through earth. From left to right the curves are for $10^{17}, 10^{18}, 10^{19}$ eV neutrinos respectively.

aperture for downward events with $\theta_n \leq 18°$ the aperture for upward going events with $\theta_z \geq 100°$ and track length greater than 50° is roughly a factor of 8 larger.

As a result of the attenuation of the upward going neutrino flux, the observation of an event with $\theta_z \geq 100°$ would accompanied by the observation of a large number of upward going events with $90° \leq \theta_z \leq 100°$ if the source is a diffuse neutrino flux. If an event is observed with $\theta_z \geq 100°$ without the attendent events at smaller $\theta_z$, then the source of event must be other than a diffuse neutrino flux. Such events would be of profound importance if observed. A general search of the data set for convincingly upward going events at all $\theta_z$ is made. It is important to note that there are a number of potential sources of spurious upward events. These include laser shots, flashers, weather distorted flashers, and whatever the army may be testing at the Dugway Proving Grounds. With this in mind, a search for upward

going events with zenith angles greater than 100° and track length greater than 50° will be made with the possible spurious sources being dealt with on a case by case basis.

# CHAPTER 5

# CANDIDATE EVENTS

The data base of monocular events from FEI that were reconstructed by the GEO routine [7] was searched for events with $\theta_n \leq 25°$. This was accomplished by first reading the event record and making a cut based on the track length and the direction of propagation. Events with track lengths greater than 30° and downward going were then examined for their $\theta_n$. Due to the manner in which GEO data are parameterized, the search range was either $0° \leq \theta_n \leq 30°$ or $150° \leq \theta_n \leq 180°$. It should be noted that a concurrent search for upward going events was made and found no upward events that met the $\theta_z$ criterion, had track lengths longer than 50°, and were not laser shots. Table 5.1 summarizes the events found in this search with $\theta_n \leq 25°$ where $\theta_n$ has been redefined to be between 0° and 90°.

As can be seen from the list of events, there are none which meet the criterion for deeply penetrating events. As a result, there can be no measurement of the flux of

Table 5.1. Events with $\theta_n \leq 25°$.

| Date | Event | $\theta_n$ |
|---|---|---|
| 2/21/82 | 119 | 24.9 |
| 7/27/84 | 2089 | 24.3 |
| 3/22/85 | 6006 | 25.0 |
| 7/10/86 | 199 | 21.4 |
| 8/2/87 | 734 | 22.0 |
| 1/12/88 | 5316 | 23.9 |
| 11/5/88 | 723 | 22.1 |
| 12/3/88 | 6 | 24.8 |
| 3/1/89 | 6930 | 21.0 |

deeply penetrating particles but the absence of such events can be used to set limits on the proposed source models. No events whose $\theta_n$ is within 2° of the requirement for deeply penetrating events. The task of the remainder of this dissertation will be to examine the implications of the nonobservation of deeply penetrating EAS.

## 5.1 Consistency Check

This is accomplished by scaling the Monte Carlo $\theta_n$ distributions by the appropriate factor and then comparing the predicted number of events with $\theta_n \leq 25°$ to the 9 actually observed. In the specific case of the epoch 4 output shown in Figure 4.6, 336 simulated events had $\theta_n \leq 25°$. Because the data represent 100 times the actual number of cosmic ray events in the real data set, the number of events with $\theta_n \leq 25°$ predicted by the simulator is 3.3. This is compared to one epoch 4 event found in the real data. Given the statistics, this is reasonably self-consistent. The first time this self-check was done in December of 1991 it was immediately apparent that there were serious problems. At that time the simulation routine predicted roughly 320 detected events in the complete data set. It quickly became apparent that in the tails of the Monte Carlo generated $\theta_n$ distribution the model did not match the data. In the course of attempting to resolve the inconsistency, a number of changes in the Monte Carlo became necessary. A brief description of the most prominent modifications in the code follows.

Early on it was discovered that a special feature of the operation of the ring 5 mirrors, namely the 3-fold local coincidence requirement, had not been implemented in the model. This was recently fixed in the general group version of the code. Unfortunately the modification took place after the version of the code used in this dissertation had been split off from the normal software support process. Implementing the 3-fold coincidence requirement had a dramatic effect on the triggering efficiency of deep events. It is important to note that the detector

simulator was in operation for 9 years before this oversight was noted and corrected. The effects of this oversight on previously published results are negligible in most cases but may have affected previous work on deeply penetrating events [5, 6].

It was also found that the standard model of the atmosphere and its aerosols implemented in the Monte Carlo code in 1980 differed substantively from more current measurements. Recent work by Luo [68] in this group and others [85, 55] suggest a more detailed model of the atmosphere is needed. A new model of atmospheric aerosols based on work by Spinhirne *et al.*[85] was included and had a significant impact on the Monte Carlo data. This modification is necessarily very preliminary and a great deal of work remains yet to be done on this topic. Cirrus clouds, along with weather in general, need to be modeled more realistically. The daily, and even hourly, variations in lower atmosphere aerosol distributions also need to be modeled. Details like the angular distribution of aerosol scattered light need to be examined in the light of more recent measurements [68].

Along with these two significant model changes a number of minor adjustments were made. These ranged from updating the noise modeling routine to introducing more current quantum efficiency files. In some cases these changes had no descernable effect on the data. There remain a number of features of the model where it is not clear what the best current model of the process is. As an example, the phase distribution of the aerosol scattering process is not consistent with the work of Luo [68] but the best choice for modeling the Dugway atmosphere is not clear. The effect of replacing the existing Monte Carlo distribution with that cited by Luo is apparent in the data. Further study is needed to resolve this issue. There remain other unresolved issues like this in the code.

The net result of these modifications is that the detector simulator yields data distributions more like the real data. In spite of the changes, the Monte Carlo still overestimates (Table 5.2) the number of events detected in the tail of the

$\theta_n$ distribution. Because the purpose of this dissertation is **NOT** to reinvent the detector simulator and there seems to be no end of small updates in the code. the introduction of a correction factor is now considered. This correction factor does no more than scale the predicted number of events in the tail of Monte Carlo data to the number of events in the tail of the real data set. Table 5.2 gives the correction factors by epoch based on the number of events seen with $\theta_n \leq 25°$. These correction factors could be used to adjust the predicted detection efficiency for neutrinos and charm matter on an epoch by epoch basis. At best this provides only an approximate correction since it is unclear whether the relative Monte Carlo performance continues to worsen as data further out in the tail is examined. It should also be noted that a systematic shift of less than 1° in $\theta_n$ between the Monte Carlo and the real data would reduce the correction factor to 1. in all epochs. This occurs because the bulk of the events with $\theta_n \leq 25°$ that triggered the detector simulator have $\theta_n \geq 24°$. Because the question of systematic shifts is not resolved, it is deemed prudent to not use the correction factor to reduce the calculated detection efficiencies at this time. The values of the correction factor are reported here in the event that they may become useful.

Table 5.2. Ratio of predicted Monte Carlo events with $\theta_n \leq 25°$ ($N_{mc}$) to the real data ($N_{real}$).

| Epoch | $N_{mc}/N_{real}$ |
|---|---|
| Epoch 2 | 1.0 |
| Epoch 3 | 1.5 |
| Epoch 4 | 3.3 |

# CHAPTER 6

# NEUTRINOS

Neutrinos from astrophysical sources were briefly discussed in a previous chapter. In all of these models the dominant process by which high energy neutrinos are created is the $p\gamma_i$ interaction. pp interactions are also a potential source of high energy neutrinos. In the case of cosmic ray nuclei at large in the universe the dominant radiation field is the 2.7° microwave background. For AGN models it is the local radiation field of the compact object. The cross section for the $p\gamma_i$ interaction turns on strongly at a photon energy around .2 GeV in the proton rest frame [86. and references therein]. In the case of cosmic ray nuclei this means that $10^3$ EeV protons interact with photons from the peak of the 2.7° blackbody radiation field. Due to the high energy Boltzmann tail of the radiation field the effect will turn on at significantly lower particle energies. The dominant branches in this process are

$$\begin{aligned} p + \gamma \rightarrow \Delta(1232) \rightarrow n + & \quad \pi^+ \\ & \hookrightarrow \quad \mu^+ + \overline{\nu_\mu} \\ & \hookrightarrow e^+ + \overline{\nu_e} + \nu_\mu \end{aligned} \tag{6.1}$$

and

$$\begin{aligned} p + \gamma \rightarrow \Delta(1232) \rightarrow p + & \quad \pi^0 \\ & \hookrightarrow \gamma + \gamma. \end{aligned} \tag{6.2}$$

Roughly 40% of the total cross section is in the neutrino producing branch. A straightforward calculation shows that the energy of all the neutrinos produced

will be of the same order. This is why most models calculate only the $\nu_\mu$ or $\nu_e$ energy spectrum and multiply by an appropriate factor to get the total neutrino spectrum. Of the three neutrinos that result from this process. $\nu_\mu$, $\overline{\nu_\mu}$, and $\nu_e$, the FE experiment is sensitive primarily to the $\nu_e$. This is due to the fact that in EHE neutrino interactions the differential cross section $d\sigma/dx_F$, where $x_F$ is the ratio of the energy of the outgoing lepton to the primary neutrino energy, is strongly peaked near $x_F \sim 1$ [82]. As discussed by Quigg *et al.*[82], this peaking is due to the growth of the quark distribution functions at small $x$ and large momentum transfer $Q^2$ in conjunction with the $Q^2$ cutoff generated by the boson propagator. (Note: Here $x$ is not the Feynman variable $x_F$ but rather the scaling variable $x=Q^2/2M(E_\nu-E_\mu)$.) The result is that in $\nu_\mu$ interactions the bulk of the primary energy is carried off in a muon that does not produce a detectable EAS.

Given this mechanism for production of astrophysical neutrinos the actual expected flux of neutrinos is dependent on specific assumptions about the spectrum of primary nuclei, evolution of the primary particle production mechanisms, and radiation fields among others. This chapter will be devoted to a qualitative examination of two models that yield predicted neutrino fluxs that are plausibly detectable. The principal purpose is to test the consistency of the nonobservation of deeply penetrating events with a given model of the EHE neutrino flux.

## 6.1 Model of C.T. Hill and D.N. Schramm

This model [58] is an extension of earlier work by other investigators [86, 89, 87, 48]. All of these authors have built on the basic process pointed out by Greisen [51] and Zatsepin *et al.*[94] that photonuclear interactions of EHE cosmic rays of extragalactic origin with the microwave background would lead to a cutoff of the cosmic ray spectrum. It was realized that along with the cutoff of the spectrum a potentially detectable flux of EHE neutrinos and photons would also

result from this process. Much of the early work in this field was directed towards analysis of the photon component of this process. Because neutrino interactions are potentially distinguishable from other particle interactions, an interest developed in the neutrino component of the cosmic ray spectrum. Neutrinos are distinguishable from other components of the cosmic ray flux by virtue of their low cross section. Deeply buried detectors can search for events initiated by particles that must have traversed path lengths in the earth that are opaque to all known particles other than neutrinos. The signature of a deeply penetrating event in the Fly's Eye data set is another means of distinguishing neutrino initiated events from others. The model of Hill and Schramm calculates the expected EHE neutrino flux from the interaction of extragalctic EHE cosmic ray nuclei with the 2.7° microwave background. Current views of the structure and evolution of the cosmos are included in this model. Other processes, such as the AGN model of Stecker *et al.*[88] or pp interactions between cosmic rays and interstellar matter, may contribute substantially to the overall neutrino flux and must be considered separately.

### 6.1.1 The Basic Model

In this model the EHE cosmic ray flux above $10^{16}$ eV is asssumed to originate in sources that are uniformly distributed throughout the universe. The propagation of the cosmic rays from a standard source through the intervening medium is found from a numerical solution to a transport equation. In this process, the secondary particles from interactions of the cosmic rays with the medium are tracked until they can no longer contribute to the production of EHE neutrinos. This is a significant difference between this work and other previous work. In the past, most analysis of cosmic ray propagation has been based on average properties of the particle interactions. Typically previous papers have modeled the propagation of the cosmic rays through a diffusion process that has not considered the effects due to secondary

particles. The resulting EHE neutrino flux at the earth from a defined standard source is calculated taking into consideration the spectrum of the 2.7° microwave background, the energy spectrum of the pions produced, and the energy of the recoil nucleon in the interactions. The neutrino flux is dependent on the distance to the source, the specific energy dependence of the cosmic rays produced by the source, the rate of production of EHE cosmic rays known as the source activity, the redshift of the source, and the assumed intergalactic and universal radiation fields.

As the redshift of a source increases so does the temperature of the universal microwave background in the reference frame of the source. This results in a lowering of the GZ cutoff energy for cosmic rays from this source. The overall efficiency of neutrino production will be increased and extended to lower energies by this mechanism. In addition, the energy of neutrinos observed from a particular source will be reduced due to redshift effects. Qualitatively this process suggests that the highest energy neutrinos will be from relatively local sources. Distant sources with higher redshifts will contribute to the EHE neutrino spectrum at lower energies. Assumptions about the density of sources as a function of redshift will affect how this mechanism contributes to the overall EHE neutrino spectrum.

In this model, the source activity is a measure of the total production rate of cosmic rays. It has been observed that the radio luminosity of galaxies increases with $z$ [67, 92, 33]. The observed radio luminosity is consistent with radiation from electrons accelerated by Fermi shock acceleration to very high energies [13]. This suggests that the charged particle acceleration environment is enhanced in galaxies with higher redshift. This in turn leads to the expectation that the acceleration of cosmic ray nuclei to EHE energies will be commensurately enhanced. The result is a relative increase in the flux of higher energy cosmic ray nuclei which yield higher energy neutrinos from a source with greater redshift. The specific form of dependence of the source activity on redshift used in this model is given in

equation 6.3. Here $z$ is the redshift and $\eta_0$ is the activity of the standard source at $z = 0$. $\bar{z}$ is the maximum redshift of sources that contribute to this model. The production mechanisms for EHE cosmic rays necessarily turned on at some point in the evolution of the universe. Astrophysical observations of extremely energetic radio source provide a possible upper limit on $\bar{z}$ neutrino flux

$$\eta(z) = (1+z)^m \theta(\bar{z} - z)\eta_0 \tag{6.3}$$

The energy dependence of the EHE cosmic rays produced by a source is taken to be of the form

$$j(E) \propto E^{-\gamma_i}(cm^2 - s - sr - GeV)^{-1}. \tag{6.4}$$

In this expression for the differential flux produced by the source, $\gamma_i$ is the injection spectral index. The power law dependence of the differential flux is a fundamental feature of measurements of the cosmic ray spectrum at high energies. Although $\gamma_i$ is not directly measured, it is a feature of the models of acceleration process that lead to the observed spectral index of EHE cosmic rays. Current measurements of the EHE spectrum find the observed spectral index to be $\gamma = 3.0$.

### 6.1.2 Spectrum Calculation

Once the local neutrino spectrum due to a standard source with $z = 0$ and activity $\eta_0$, at a distance $R_0$, has been calculated then the total spectrum can obtained by integration over all sources. This integration includes previously discussed direct redshift and source activity effects. In addition the density of sources has the following dependence on the redshift due to the expansion of the universe.

$$\rho(z) = (1+z)^3 \rho_0 \tag{6.5}$$

In this expression $\rho_0$ is the density of sources at $z = 0$. The resulting unnormalized total neutrino spectrum has a number of free parameters. These include $\bar{z}$, the

maximum redshift, $\bar{z}$. the injection spectral index. and $m$, the source activity exponent. Current limits on $\bar{z}$ are set by astrophysical observations of quasars. $\bar{z}$ is currently thought to be in the range of 2-4 [39] based on these observations. $\gamma_i$ is expected to be near 2.0. This is a typical spectral index calculated by models of EHE cosmic ray acceleration from 1st order Fermi shock acceleration. This is also consistent with the injection spectral index used in models [10, 15] which predict the $\gamma = 3.$ spectral index of EHE cosmic rays. Measurements of the radio luminosity of highly redshifted sources indicate that there is an increase in the luminosity with increasing redshift. At $z$ near $\bar{z}$, it is unclear whether the luminosity of higher $z$ sources decreases or if the density of such sources decreases. Either scenario could account for the observations. In this model of neutrino production, it is assumed that the source luminosity has the form given in 6.3 and that the cutoff in $z$ is due to effects other than a loss of luminosity in highly reshifted sources. At the time this model was proposed, there was some evidence for $m$ in the range of 4-5 [83]. More current measurements in the x-ray region suggest $m$ is roughly 2.6.

The remaining task is to normalize the calculated spectrum. In the case of this model, it is accomplished by tying the EHE cosmic ray particle spectrum calculated by Hill and Schramm to an observed EHE spectrum. Because the particle and neutrino spectra are directly related this provides the normalization for the neutrino spectrum as well. The spectrum published by the Haverah Park collaboration [36] was chosen given that is was the most statistically significant available at the time of this paper.

Figure 6.1 shows the resulting EHE neutrino spectrum and illustrates the $\bar{z}$ dependence of the model for $\gamma_i = 2.0$ and $m = 4.5$. The activity index does not play a role in the asymptotic spectral slope but rather affects the flux levels for the different $\bar{z}$. $\gamma_i = 2.0$ was found to give the best fit to the Haverah Park data, which are consistent with previous models of the EHE particle spectrum. It should

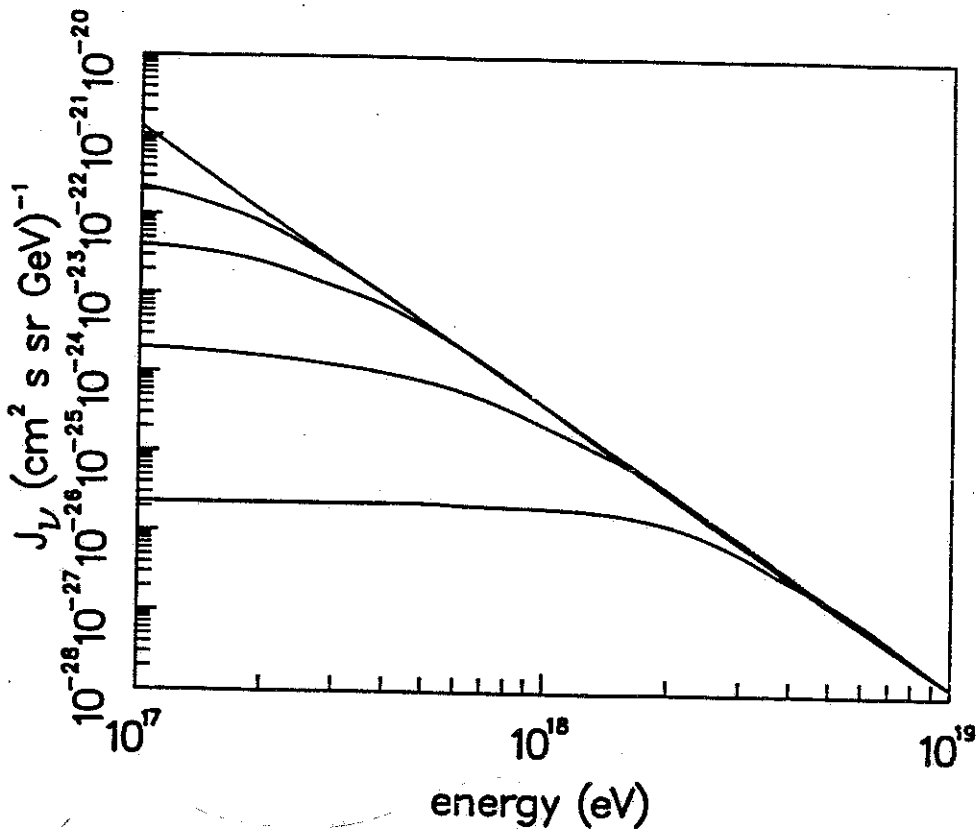


Figure 6.1. The predicted differential neutrino spectrum above $10^{17}$ eV as a function of $\bar{z}$, the maximum redshift. $\gamma_i$ is 2.0 and $m$ is taken to be 4.5. From bottom to top the different curves represent $\bar{z}$= 2, 4, 6, 8, and 10 respectively. This spectrum is normalized to the Haverah Park EHE cosmic ray particle spectrum.

be noted that the spectrum as presented in the original paper is incorrectly drawn and has been corrected here.

### 6.1.3 Calculation of Expected FE Neutrino Events

The quantity that must be detemined in order to calculate the number of deeply penetrating events is the energy dependent aperture function. Qualitatively, this represents the detection efficiency for neutrinos that enter the fiducial volume of the detector and meet the criterion for a deeply penetrating event. This function, denoted by $\Omega(E)$, together with the detector on-time and the proposed neutrino spectrum are used to calculate the expected number of detected events in some

energy window. The consistency of this calculated value with the actual number of detected events may then be evaluated. This portion of the dissertation will describe the principal features of the calculation of the aperture function and the expected number of detected events. The actual procedure by which this is accomplished in terms of computer code, batch files, and plotting routines is documented in appendices to this document.

The process begins by generating a set of random EAS trajectories that isotropically and homogeneously fill the space of possible arrival directions. These EAS are assigned a particular energy in the energy interval $10^{17}$ eV to $10^{20}$ eV. The low end of this window is defined by the turn on of detector sensitivity and the high end by a combination of atmospheric transparency and the rapidly falling cosmic ray or neutrino spectrum. Once the trajectories, or tracks, are generated, those that meet the geometric criterion of a deeply penetrating event as established in Chapter 4 are selected to be passed on to the next step in the process.

For each trajectory generated the total amount of matter traversed by the neutrino is calculated. Given the low cross section for neutrinos [82] interacting with air the probability of given neutrino generating an EAS within the fiducial volume of the FE is small. For the same reason, if the neutrino does initiate a shower, it will do so at any point along its track with equal probability. If a careful statistical approach were folllowed in this process, a number of event trajectories would have to be generated to find even a few that resulted in the initiation of an EAS. This would hopelessly bog down the computational process. To improve the efficiency of the calculation, the neutrino is 'forced' to interact at some random point along its path. The event is then weighted by the probability that it would have interacted somewhere along that track.

Once the point of initiation of the EAS is determined, this information along with the shower trajectory and energy is passed to the detector simulation program.

The simulator then determines whether each event would trigger the detector. In this case it is assumed that the EAS is initiated by an electron that leads to a parameterization of the number of particles in the shower at a point along the track given by Hillas [57]. Events that trigger the detector are then passed to the next stage.

The monoenergetic aperture, $\omega_E$, is calculated as follows.

$$\omega_E = \{A \cdot \sum_{i=1}^{n} \sigma_{\nu N} N_A G_i\}/N \tag{6.6}$$

In this expression A is the detector fiducial volume that is given by $\pi R^2 \cdot 2\pi \ m^2 - sr$ where $R$ is the maximum impact parameter with which the original trajectories were generated. $N_A$ is Avogadro's number and $G_i$ is the column thickness (g/cm$^2$) along the trajectory. $N$ is the number of tracks generated in the first step of this process. The sum is over the $n$ simulated events that triggered the detector Monte Carlo, were successfully reconstructed, and satisfied the criterion for deeply penetrating events. The quantity being summed, $\sigma_{\nu N} N_A G_i$, is the probability that the neutrino will interact with the atmosphere during its traversal of the fiducial volume of the detector thereby initiating an EAS. The neutrino cross section, $\sigma_{\nu N}$, is from the recent work of Reno and Quigg [82]. This $\sigma_{\nu N}$ is larger, especially at the highest energies, than the cross section used in previous calculations of the UHE neutrino flux [4, 7]. Once $\omega_E$ has been calculated for a number of energies a polynomial fit to these monoenergetic apertures is performed to generate $\Omega(E)$.

Predictably, $\Omega(E)$ is dependent on the detector configuration which has evolved with time as in any large experiment. The FE detector has experienced five major optical and electronics changes over its current lifetime although only four are covered by this dissertation. As a result, $\Omega(E)$ should more properly be written as $\Omega_e(E)$ where $e$ labels the epoch of detector performance between 1 and 4. The specific dates and detector configurations associated with each epoch are well

documented by K. Green [50] and will not be repeated here. The detector simulator can be switched to any of the system configurations required to calculate all the $\omega_E$'s needed to generate the different $\Omega_e(E)$'s.

After all the $\Omega_e(E)$'s are known, the number of deeply penetrating events expected due to any cosmological neutrino spectrum can be calculated. The number of expected events in an energy window $[E_1, E_2]$ is given by equation 6.7.

$$N(E_1, E_2) = \sum_{e=1}^{4} \tau_e \int_{E_1}^{E_2} \Omega_e(E) n(E) dE \tag{6.7}$$

where

$$\begin{aligned} N(E_1, E_2) &\Leftrightarrow \text{expected events between } E_1 \text{ and } E_2 \\ \tau_e &\Leftrightarrow \text{detector on time for epoch } e \text{ (s)} \\ \Omega_e(E) &\Leftrightarrow \text{aperture for epoch } e \text{ (cm}^2\text{-sr)} \\ n(E) &\Leftrightarrow \text{differential } \nu \text{ flux } (\text{(cm}^2\text{-s-sr-GeV)}^{-1}) \end{aligned}$$

Note that the sum over epoch dependent terms may be taken inside the integral. This sum is then a total time weighted aperture, $\Omega(E)$, and is shown in Figure 6.2. Table 6.1 gives the expected number of deeply penetrating events over the $2.1 \cdot 10^7$ s of detector on time based on the neutrino spectrum of Hill and Schramm shown in Figure 6.1. As can be seen, the number of events expected depends on the assumed $\bar{z}$. Even for $\bar{z}$ greater than that suggested by current observations there is still no expectation of observed events from this source. The table shows that nonobservation of deeply penetrating events by the FE experiment is consistent with this model of the EHE neutrino flux.

## 6.2 AGN Model of F. Stecker *et al.*

This model [88] proposes Active Galactic Nuclei, AGN, as sources of a diffuse EHE neutrino flux. The magnitude of this flux is of the same order as that predicted by the model of Hill and Schramm. Although the bulk of the flux due to this proposed mechanism is at energies below the FE threshold the high energy tail is still plausibly detectable. The expected number of deeply penetrating events due to

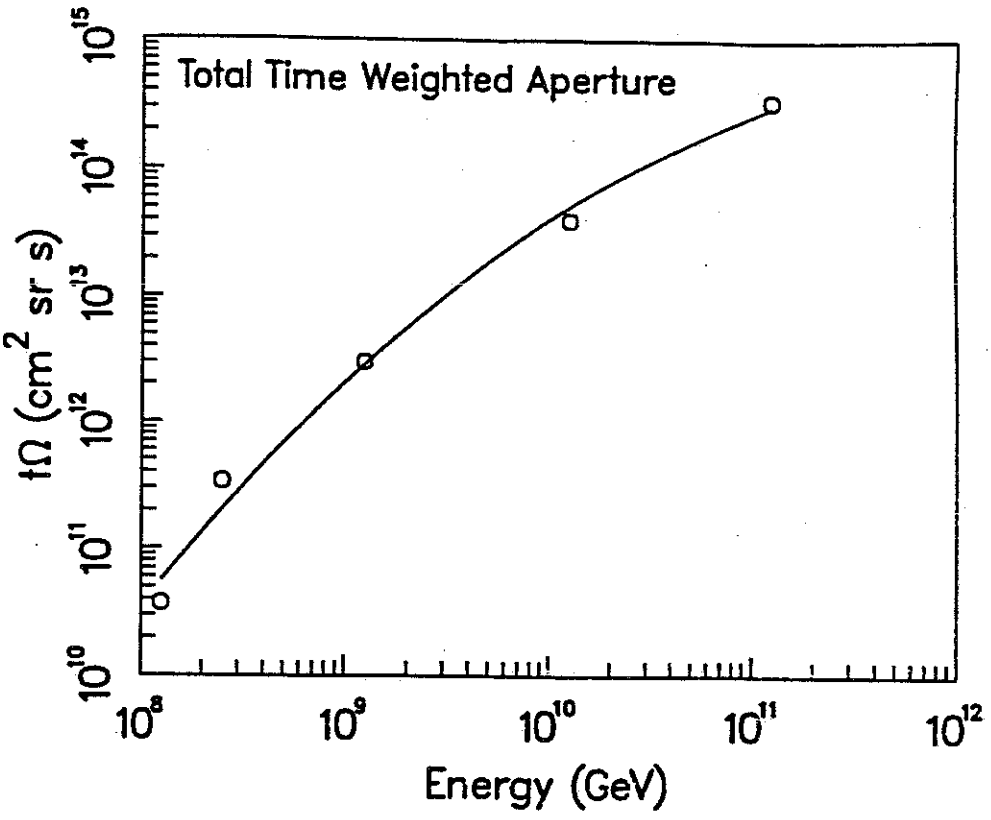


Figure 6.2. Total time weighted aperture as a function of energy. $\Omega(E)$ given by $\sum_{e=1}^{4} \tau_e \Omega_e(E)$. Total detector on time represented is $2.1 \cdot 10^7$ s.

Table 6.1. Expected number of deeply penetrating $\nu_e$ events detected by FE experiment due to neutrino spectrum proposed by Hill and Schramm as a function of $\bar{z}$.

| Neutrino Events | |
|---|---|
| $\bar{z}$ | Number Expected |
| $\geq 10$ | $6.16 \cdot 10^{-3}$ |
| 8 | $5.47 \cdot 10^{-3}$ |
| 6 | $3.39 \cdot 10^{-3}$ |
| 4 | $1.23 \cdot 10^{-3}$ |
| 2 | $3.76 \cdot 10^{-4}$ |

AGN neutrinos is obtained by employing the AGN neutrino spectrum in equation 6.7. All other features of the calculation are identical. Before presenting this result the salient features of the model of Stecker *et al.*will be discussed.

As the most powerful emitters of radiation known, AGN are candidate sources for EHE particles of all types. There are two features of AGN that are pertinent to this model of EHE neutrino production. These are the proposed accretion shock at some distance from the massive black hole that powers the AGN and the observed UV and x-ray spectra. Fermi acceleration at the accretion shock is expected to produce a significant number of EHE nuclei with a characteristic $E^{-2}$ spectral dependence. These ultra-relativistic particles will interact with the local radiation field and particle environment yielding extremely energetic secondaries. Observations of the AGN x-ray spectra suggest that the column density of matter is relatively low where the x-rays are produced. This sets upper limits on the amount of matter available for pp interactions. The rapid time variability of the x-ray emission indicates that the x-ray production region is smaller than the production region of the UV portion of the photon spectrum. The resulting large photon density at the core of the AGN leads to $p\gamma$ interactions dominating pp interactions. Using a standard model for AGN, this paper calulates a EHE proton spectrum due to accretion shock acceleration. From this particle spectrum and the observed photon density, a secondary neutrino spectrum is calculated for a standard AGN source. As in the previous model, this standard source is then integrated over the observed density of such sources in the universe with appropriate corrections for cosmological effects. The result is the total diffuse differential neutrino spectrum shown in Figure 6.3.

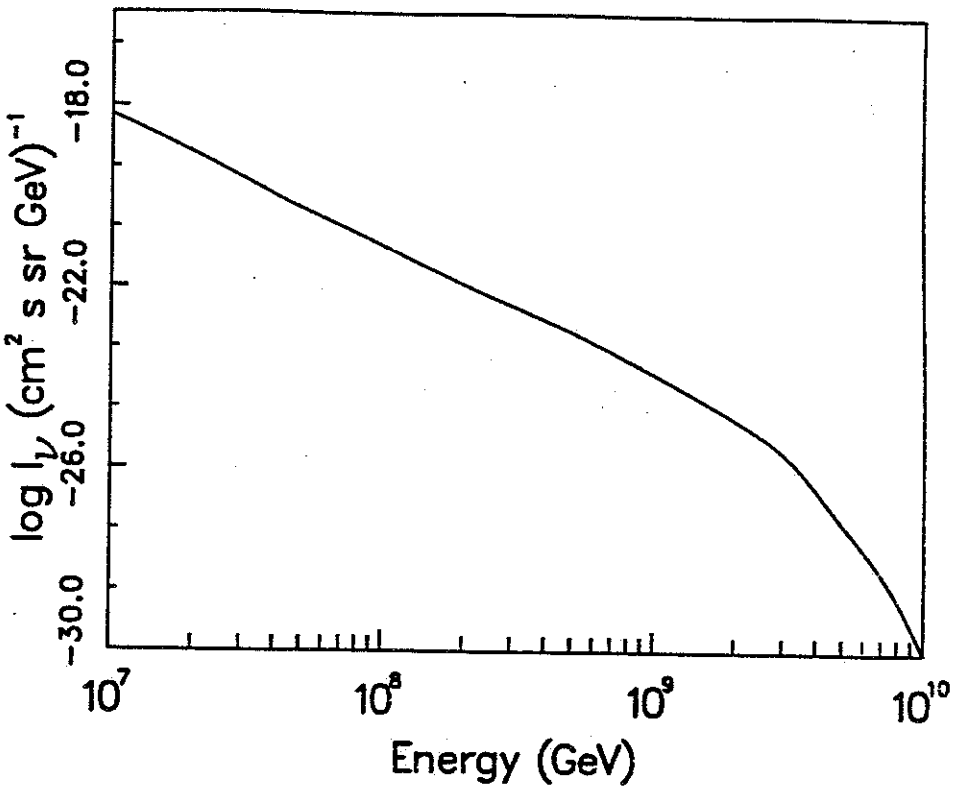


Figure 6.3. AGN differential neutrino spectrum from diffuse AGN sources as calculated by F. Stecker *et al.*.

### 6.2.1 Expected AGN Events

The result is that $8.89 \cdot 10^{-3}$ events are expected with energies greater than $10^{17}$ eV. This is consistent with the nonobservation of candidate events by the FE experiment.

## 6.3 Conclusions

The fundamental conclusion of this portion of this dissertation is that the results of a search for deeply penetrating events in the FE data lead to no contraints on current models for the production of cosmological neutrinos. In the event the aperture function can be increased by ~1000, then there is a real possibility that neutrino induced deeply penetrating events will be detected. This is not unrealistic given the HiRes detector currently under construction [59].

# CHAPTER 7

# CHARM QUARK MATTER

In Chapter 4 a qualitative argument was given for the consideration of charm quark production as a mechanism for the production of deeply penetrating EAS. In this chapter the nonobservation of deeply penetrating events will be compared to the number of deep events expected based on the predicted characteristics of charm production at $\sqrt{s} \geq 15$ TeV. Where possible the various parameters needed to model the production and propagation of charm quark matter will be taken from experimental results or theoretical predictions in the literature. In some cases this is not possible so a 'reasonable' value or form is assumed.

There are many steps between the production of a charmed hadron or meson in the interaction between a primary cosmic ray and the atmosphere and the detection of a deeply penetrating EAS directly attributed to that charmed particle. Table 7.1 is a description of the discrete stages in that process. An observation of deeply penetrating events due to charm production necessarily addresses the combined effect of all these processes. Such an observation can not be used to directly determine any single parameter of the charm production and propagation process. Because a model of this process will be more sensitive to certain parameters than others, it is to be hoped that useful constraints can be derived. It is the purpose of this portion of the dissertation to determine these constraints.

Due to the significantly heavier masses of the bottom and top quarks, 4.7 GeV/$c^2$ and $\sim$ 100 GeV/$c^2$ respectively, relative to charm, 1.5 GeV/$c^2$, the expectation from QCD [9, 74] calculations is that the total hadronic production cross section for these quarks will be substantially reduced from that of charm quarks. Bottom production

Table 7.1. Stages in charm quark production of deeply penetrating events.

| | |
|---|---|
| 1 | production of charm quark matter depends on total cross section for $pN \rightarrow c\bar{c} + X$ |
| 2 | energy of charm matter produced depends on differential cross section with respect to $x_F$, Feynman x |
| 3 | propagation of charm matter through the atmosphere depends on several parameters. These are; i) cross section of charm matter with air ii) elasticity distribution of interactions in i) iii) charm matter lifetime |
| 4 | energy deposited along event track in small EAS due to recoil particle from 3ii) above must be tracked |
| 5 | charm matter decays and standard hadronic EAS is initiated |
| 6 | recoil shower from 4) together with EAS from 5) is (isn't) detected by FE |

is expected to be reduced by a factor of 10 relative to charm while top production is predicted to be a factor of 100 lower. An additional consequence of the mass of the bottom is that the relativistic $\gamma$ for bottom matter is reduced by a approximately 3 from that of charm matter of equal energy. This reduces the lab lifetime of bottom matter and hence the probability of the particle's decay energy being deposited deep in the atmosphere. For these reasons, the question of detection of deeply penetrating EAS initiated by bottom or top matter will be tabled until the same question is resolved for charm matter.

## 7.1 Charm Matter Characteristics

There are two basic problems in establishing the nature of the parameters that effect the production and propagation of charm matter at EHE energies. The first is that there is no accelerator data at energies anywhere near the EHE range. In recent years, the highest energy measurements of the total inclusive charm production cross section ($\sigma_{c\bar{c}}^{tot}$) have been in the range $\sqrt{s} = 60$ GeV [37]. This

is nearly 3 orders of magnitude below the FE regime. This means predictions of $\sigma_{c\bar{c}}^{tot}$ must be extrapolated a long way in the absence of constraining data. The other problem is that the mass of the charm quark at $\sim$ 1.5 GeV is not large enough to permit the application of perturbative QCD to the calculation of charm properties. Unfortunately, there is no other choice of methodology, which means that predictions of charm production are assumed to be fraught with uncertainty [74]. As a result, the charm parameters in the literature must be considered as qualitative rather than quantitative predictions.

With this in mind, the predicted charm parameters affecting the production and detection of charm initated EAS will now be individually discussed.

### 7.1.1 Total Charm Production Cross Section, $\sigma_{c\bar{c}}^{tot}$

Included in the question of $\sigma_{c\bar{c}}^{tot}$ is also the issue of the differential cross section with respect to $x_F$, $d\sigma^{tot}/dx_F$. In both cases the experimental data and the theoretical predictions have not yet been reconciled.

In the case of $\sigma_{c\bar{c}}^{tot}$, the empirical result is that the cross section rises much more quickly with energy than theoretically predicted [37]. Because these results must be extrapolated from $\sqrt{s} = 60$ GeV to $\sqrt{s} = 15$ TeV, the ability to accurately predict the results at lower energies is very important. Barger *et al.*[9] have proposed a model for charm production that yields a prediction (Figure 7.1) for the total cross section given $m_c = 1.5$ GeV. In cases where the models of charm production do not agree with the empirical data the model typically underestimates the cross section at high energies. In the case of the model of Barger *et al.*, if the model is extrapolated from $\sqrt{s} = 2$ GeV to $\sqrt{s} = 20$ GeV it is estimated that $\sigma_{c\bar{c}}^{tot}$ is 1 mb which is roughly 1% of the p-air cross section [25]. Because of the uncertainty of this extrapolation the total charm production cross section is taken to be a free

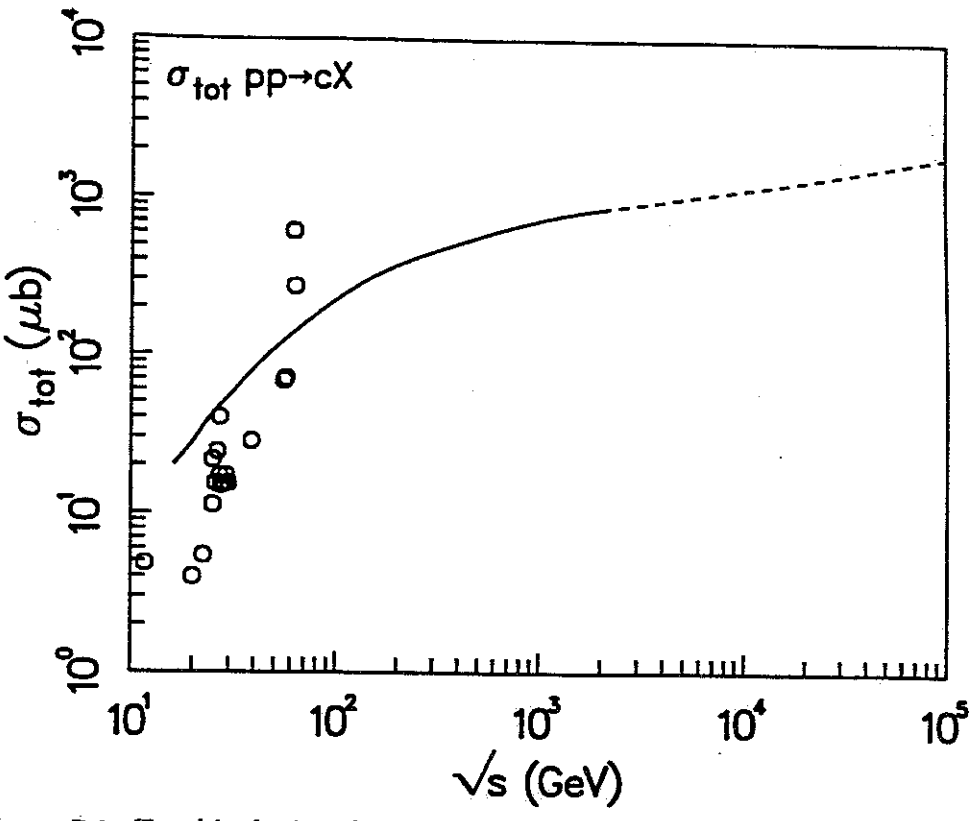


Figure 7.1. Total inclusive charm production cross section from the model of Barger *et al.*(solid line). Points indicate experimental results. Dotted line is extrapolation to higher energies.

parameter of the process with a value in the neighborhood of 1% of the p-air cross section. As will be seen later, the results of this chapter simply scale with $\sigma_{c\bar{c}}^{tot}$.

The question of the differential cross section $d\sigma^{tot}/dx_F$ is a good deal more uncertain from an experimental point of view. Historically this issue was brought to light when early measurements of the production and decay of the $D^{\pm}$ meson found unexpectedly large cross sections for the production of D at large $x_F$ [61, 1, 2, 27]. Subsequently, other experiments [43, 3] found much lower cross sections for charm production at large $x_F$. To date, the empirical evidence in this matter is still mixed leading to two distinct sets of models. The first, characterized by the work of Barger *et al.*[9], predicts a 'hard' $x_F$ distribution (Figure 7.2). The second, characterized by the recent work of P. Nason [74], predicts a very 'soft' $x_F$ distribution (Figure 7.3). Quantitatively these models of $d\sigma/dx_F$ are normally represented as having

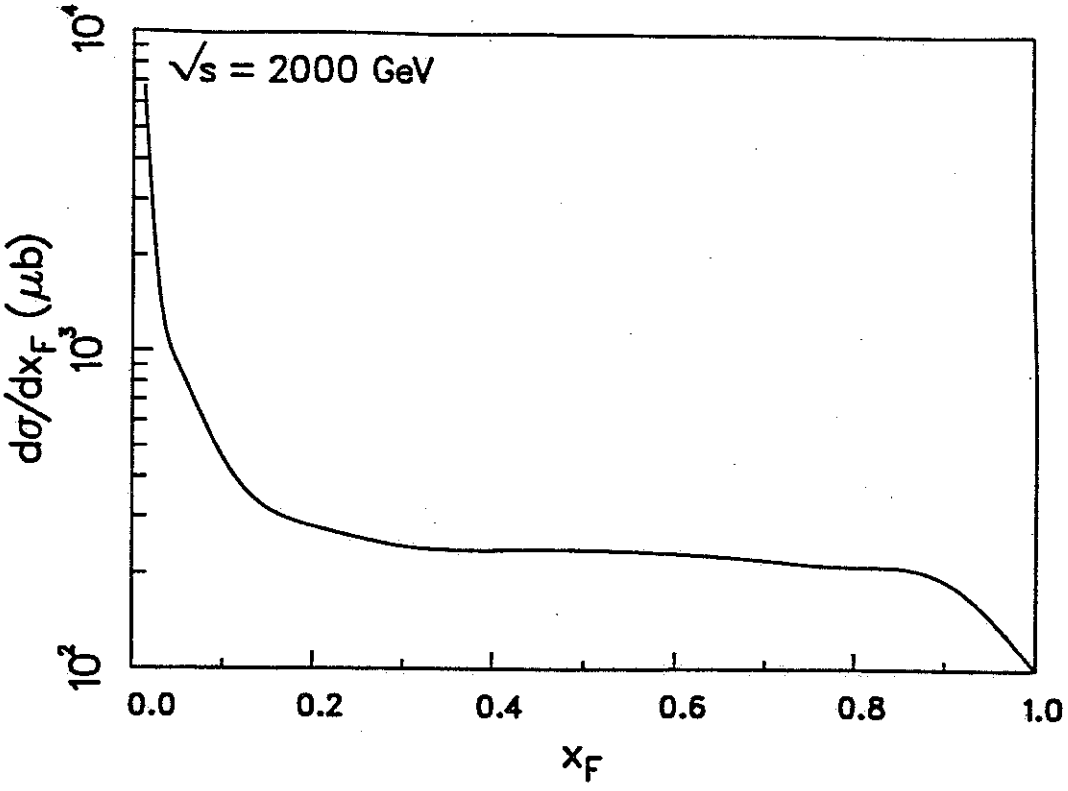


Figure 7.2. $d\sigma/dx_F$ from Barger *et al.*for the production of charm at center of mass energy equal 2 TeV.

the same functional form but with distinctly different power law dependence. As can be seen from equation 7.1 the soft $x_F$ distribution is very soft.

$$d\sigma/dx_F(x_F \geq 0.1) \propto \left\{ \begin{array}{ll} (1-x_F)^n & 1 \leq n \leq 2 \text{ 'hard' distribution} \\ (1-x_F)^n & 5 \leq n \leq 8 \text{ 'soft' distribution} \end{array} \right\} \qquad (7.1)$$

This question of the power law dependence of the differential cross section is potentially one of the more testable features of models of charm production in the context of deeply penetrating events in the FE data set. As will be seen later, a hard $x_F$ distribution leads to a charm matter flux that is much more detectable than that resulting from a soft distribution.

The basic feature of models that predict a hard $x_F$ distribution is the inclusion of a diffractive component to the charm production process. Diffractive production of charm has been much discussed in the literature [49, 54, 12, 71, 76, 11]. Diffractive processes such as $qc(sea) \rightarrow qc(valence)$ and $gc \rightarrow gc$ are distinct from central

motion of the constituent quarks of the hadron is the same the bulk of the total hadronic momentum will be carried, on average, by the heaviest quark. When this intrinsic charm state is excited and dissociated from the incoming hadron the resulting leading charm particle will have a rather hard $x_F$ distribution. It has been proposed that if $\sim 1\%$ of pp interactions resulted in production of charm via this mechanism then the hard $x_F$ empirical data could be explained. Fortuitously, the predicted contribution to the proton structure functions from intrinsic charm states is also at the 1% level. Until the empirical evidence converges, the question of diffractive production of charm in the context of production of charm at large $x_F$ will continue to be considerably confused. Because the FE experiment is sensitive only to charm production at large $x_F$, there is an opportunity to provide some important empirical input into the whole discussion.

### 7.1.2 Cross Section of Charm Matter with the Atmosphere

Once again there are two inportant issues contained in this topic. The first is the question of the inelastic cross section of charm matter with nucleons. Specifically, the cross section with air is of interest. The second question is the elasticity distribution of such interactions. The literature is sparse and not very definitive with regard to these questions. The following discussion attempts to place the assumed $\sigma^{inelas}_{c\bar{c}-N}$ and elasticity distribution into context.

In regard to the charm-air cross section, the statements from theorists run from those who expect $\sigma_{c\bar{c}-N}$ to be the same as $\sigma_{p-N}$ [63] to those who expect it to be substantially reduced relative to $\sigma_{p-N}$ [72]. In both cases the expectations are unsubstantiated. A naive use of a bag model suggests that charm matter is slightly more localized than normal hadronic matter, which would result in a slight lowering of $\sigma_{c\bar{c}-N}$ but this would not be more than a factor of more than 2-4 [38, 18].

As can be seen there is no clear concensus on the question of $\sigma_{c\bar{c}-N}$ and as a result this parameter has been left essentially free for the purposes of this dissertation. There is no reason to expect it to be greater than $\sigma_{p-N}$, which is used as an upper bound. Because it is more useful in conceptuallizing the experimental situation, the actual free parameter in the calculation is $\lambda_c$, the charm-air interaction length, which is given by $\lambda_c(\mathrm{g/cm^2} = 23.6/\sigma_{c\bar{c}-N}(\mathrm{barns}))$.

The literature regarding the elasticity distribution for charm-air interactions is extremely limited and there is no experimental work addressing this question. On one hand there seems to be no obvious reason why the elasticity distribution would be dramatically different from that of protons at EHE energies. In this energy regime, protons have an average elasticity on the order of .8 [75]. On the other hand, if the charm quark of the leading charmed hadron participates in a 'spectator' fashion then it is reasonable that the leading particle carries off most of the energy. This is due to the hard $x$ distribution of the charm quarks in the structure functions. Perhaps this is the reason for the unsupported statement by Khodjamirian [63] that the expected elasticity distribution for charm interactions would have a mean value of 0.1. In the absence of any clear direction from the literature, the elasticity distribution is also taken to be a free distribution. For the purposes of this dissertation elasticity distributions were constructed that had a given mean value. Bimodal distributions were not considered. A typical distribution with a low mean value is shown in Figure 7.4.

### 7.1.3 Charm Particle Lifetimes

The lifetimes of the various charmed particles are well known, and are given in Table 7.1.3. There are other charm particles that are surely produced in the interactions under investigation in this dissertation but their lifetimes are all roughly six orders of magnitude smaller. These particles decay so quickly that showers con-

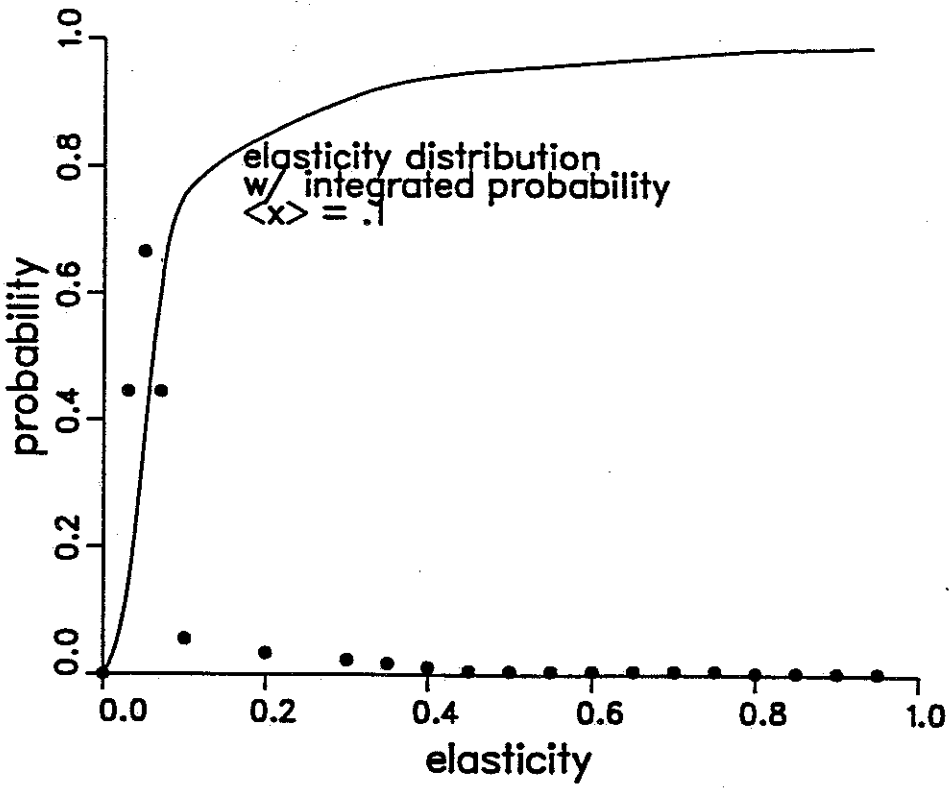


Figure 7.4. Trial elasticity distribution for charm-air interactions.

Table 7.2. Charm particle lifetimes for potentially detectable hadrons.

| Particle | Lifetime (s) |
|---|---|
| $\Lambda_c$ | $2{\cdot}10^{-13}$ |
| $D^{\pm}$ | $9{\cdot}10^{-13}$ |
| $D^0$ | $4{\cdot}10^{-13}$ |
| $F^{\pm}$ | $3{\cdot}10^{-13}$ |

taining them are indistinguishable from normal EAS. In some cases, the principal decay products of these short lived charmed particles are themselves D mesons and as such will contribute to the development of deeply penetrating EAS.

The question that arises once the lifetimes are known is what are the branching ratios in the production of charm? Because this effect is so simple to factor in after the fact no a priori assumptions about branching ratios are made. The particle lifetime is taken as a free parameter between .1 and 1 ps and branching ratio effects may be taken into account after the detection efficiencies have been calculated.

## 7.2 Charm Propagation Model

The following is an overview of the process by which the propagation of charm matter through the atmosphere was modelled. It is intended to make apparent the effects of the various free parameters on the model. These parameters are adjustable to allow for different a priori assumptions. The process by which the combined effects of the recoil showers, generated by interactions of the charm matter with the atmosphere before charm decay, and the charm decay shower are included is also described. No attempt is made to be exhaustive in this discussion. Additional information about how to actually run the programs to generate the desired results is contained in the appendices. Details of the code for this model must be sought in the code itself, which is well-documented internally.

### 7.2.1 Basic Monte Carlo

Much of the process of modeling the propagation of charm particles is similiar to the process already described for neutrinos. It begins with the generation of a set of random EAS trajectories that isotropically and homogeneously fill the available arrival directions. Those event trajectories that meet the criterion for a deeply penetrating shower are identified. For these tracks, the point at which the

primary cosmic ray, assumed for now to be a proton, interacts with the atmosphere is identified. It is assumed that a leading charm particle is produced in the initial interaction. The charm particle is assumed to have a particular energy and its lifetime is selected from an exponential distribution with a predetermined mean. Each event is then passed to an atmospheric propagation routine.

At this point an interative process is begun. Based on a preselected charm interaction length, the depth penetrated before the next charm-air interaction is generated. The depth in the atmosphere of this interaction is saved and the energy deposited in the recoil shower is selected from a specified elasticity distribution. The particle is checked to see if it has decayed and if not the current charm particle energy is saved and the process returns to calculate the depth penetrated to the next charm-air interaction. The iterations continue until the charm particle decays, at which point the energy dumped into the decay shower is stored. If the particle 'hits' the ground before decaying, the recoil data are still saved.

Following the interative propagation of the charm particle, an event shower profile that includes the recoil showers as well as the decay shower is calculated. At each collision point producing a recoil shower, a standard hadronic shower of appropriate energy is begun. A standard hadronic shower is also begun at the charm particle decay point. The accumulated number of shower particles at discrete points along the track is then found and the resulting total shower profile is saved. This shower profile is then passed, along with the trajectory information, to the detector simulator decribed in the previous chapter.

Once the number of detected particles is known, the detection efficiency for charm particles with a given energy, mean lifetime, interaction length, and elasticity distibution is determined. The detected showers also meet the previously defined criterion for deeply penetrating events. There only remains to rerun the calculation for all the desired choices of parameters and distributions. It should be noted that

not all the free parameters in the production and propagation of charm matter turn up in this portion of the calculation. The result of all theses calculations is a matrix of trigger efficiencies that depend on a number of free parameters. The aperture function, $\Omega_e(E)$, as defined in the previous case for neutrino induced events, is the fiducial volume multiplied by the trigger efficiency; that is, the primary particle flux multiplied by the charmed hadron production rate and the aperture function gives the actual detection rate.

## 7.3 Expected Charm Events

The calculation of the expected number of deeply penetrating charm events proceeds in a similiar fashion to that for the neutrino case. Equation 7.2 gives the expression that must be evaluated. It should be noted that the dependence of the aperture function on the free parameters previously mentioned is not explicitly displayed.

$$N(E_c^1, E_c^2) = \sum_{e=1}^{4} \tau_e \int_{E_c^1}^{E_c^2} \int_{E_p^{lo}}^{E_p^{hi}} \kappa C_{x_F} (1 - x_F)^n n(E_p) \Omega_e(E_c) dE_p dE_c \tag{7.2}$$

where

$N(E_c^1, E_c^2)$ $\Leftrightarrow$ expected events between $E_c^1$ and $E_c^2$
$\tau_e$ $\Leftrightarrow$ detector on time for epoch $e$
$\Omega_e(E)$ $\Leftrightarrow$ aperture for epoch $e$
$n(E_p)$ $\Leftrightarrow$ differential EHE cosmic ray flux
$\kappa$ $\Leftrightarrow$ fractional leading charm production
$C_{x_F}(1 - x_F)^n$ $\Leftrightarrow$ normalized $x_F$ distribution

The physical interpretation is easier to see if it is noted that the integration shown in equation 7.3 is just the differential spectrum for detectable charm matter. That is to say, charm matter with $x_F \geq .1$, which is variously labelled leading or diffractive charm production.

$$n(E_c) = \int_{E_p^{lo}}^{E_p^{hi}} \kappa C_{x_F} (1 - x_F)^n n(E_p) dE_p \tag{7.3}$$

Given the aperture function that is calculated for charm matter with a range of mean lifetimes, interaction lengths, and elasticity distributions, this integral is

numerically evaluated. Different choices for the index of the power law dependence of the $x_F$ distribution, $\kappa$, and the EHE cosmic ray spectrum will affect the number of events expected. In this work, the EHE cosmic ray spectrum is taken to be a known quantity based on current work of the FE group [50] and the Akeno group [64]. Because of the number of loosely constrained parameters, the results form a matrix of dimension five. The five 'free' parameters are the mean charm lifetime, the charm air cross section or interaction length, the elasticity distribution for charm-air interactions, the functional form of the differential cross section relative to $x_F$ for the production of charm, and the fraction leading charm production, which is the total cross section for the production of leading charm, as previously defined, relative to the p-air cross section. Because the expected number of events scales directly with $\kappa$ the results presented will all include an explicit $\kappa = .01$ dependence. The results of the calculation are presented in the following series of plots.

The general features of the plots can be summarized in a number of statements. First, the detectability of charm increases with longer charm interaction length and longer charm particle lifetime. Second, differential charm production cross sections with harder $x_F$ distributions result in an increased probability for detection. Because preliminary calculations showed that inelasticity distributions with means larger than .1 had even fewer expected events than those shown in the Figures 7.5 and 7.6 these data are not shown. It must be noted that even for the most optimistic choice of parameters, we find that no deeply penetrating events are expected to be seen.

## 7.4 Conclusions

We conclude that the limits that can be set on parameters that affect the production and propagation of charm matter at EHE energies from this work do not constrain existing models of these processes. Although this is unfortunate, there are

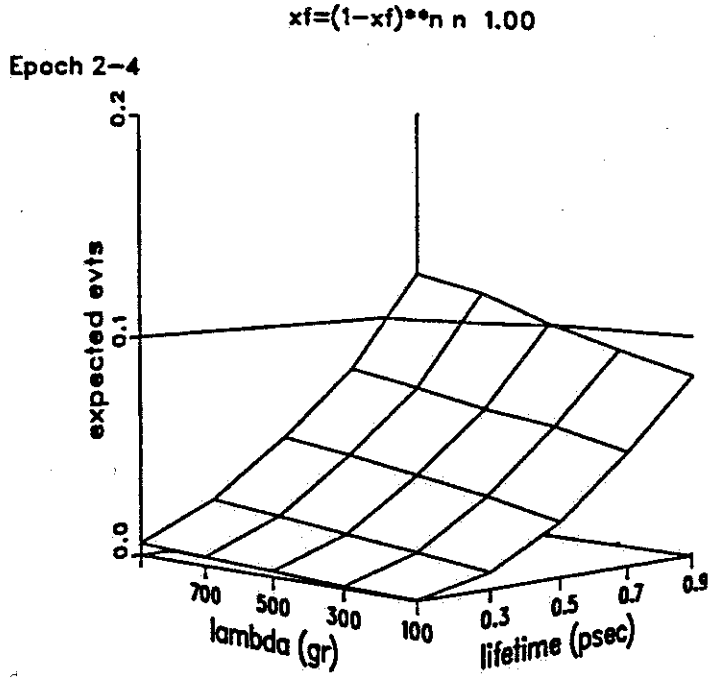


Figure 7.5. Expected charm events from a hard $x_F$ distribution as a function of charm particle lifetime and charm interaction length. An elasticity distribution with mean equal .1 is assumed.

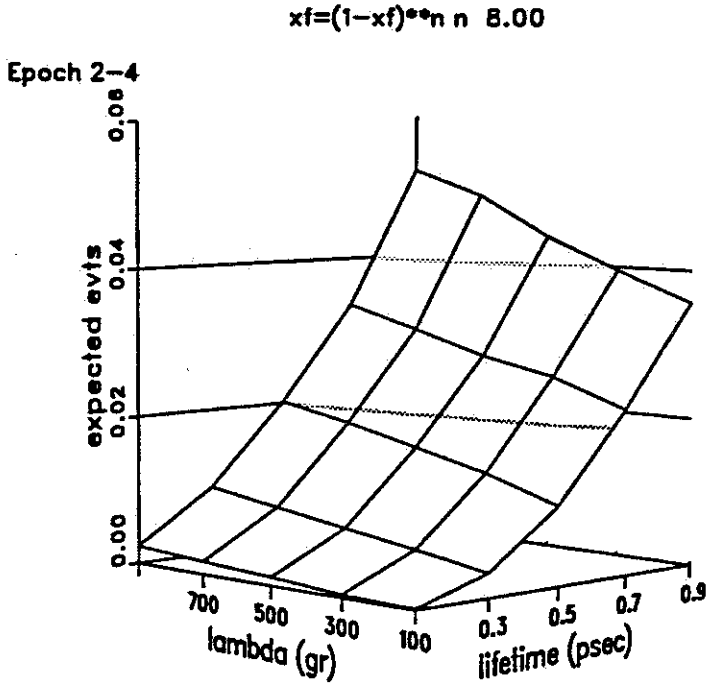


Figure 7.6. Expected charm events from a soft $x_F$ distribution as a function of charm particle lifetime and charm interaction length. An elasticity distribution with mean equal .1 is assumed.

a number of useful points to be made. The first is that although no charm events were seen or expected, an improvement of 10 to 100 in the aperture function for this process would lead to the expectation of observing events in some scenarios. This is not an unreasonable expectation in view of detectors currently under construction [59]. Secondly, for detectors with improved resolution the longitudinal shower profile of charm events may be distinguishable from that of standard events. This is the classic search for bumpy shower profiles that are characteristic of a significant subset of the charm events. It provides an additional means of investigating charm in EHE EAS. Finally this result does not suggest that current models of charm production are way off base. There is no dramatic turn on of a new and unsuspected charm production mechanism at EHE energies.

# CHAPTER 8

# EVENT SOURCE DISCRIMINATION

In the event that a deeply penetrating EAS should be detected, the question of the source of the deeply penetrating event is this immediately brought to the fore. The possibility that at some time an event may be detected that meets the established requirement of $\theta_n \leq 18°$ must be considered. The outline of a method, resulting from the work in this dessertation, for evaluating the possible source of an observed deeply pnetrating event is presented.

## 8.1 Decoupling Neutrino and Charm Apertures

As can be seen from Figures 8.1 and 8.2, the aperture functions for neutrino and charm induced deeply penetrating EAS have different $\theta_n$ dependences. Qualitatively this is a due to the fact that neutrino initiated EAS are equally probable at all atmospheric depths while charm EAS are more probable at shallower depths. It is proposed that this difference in $\theta_n$ dependence can be exploited to address the question of the source of deeply penetrating events. Based on a more careful calculation of the differential apertures, which are also strongly dependent on shower energy, the probability that an event with a measured $\theta_n$ is due to a particular source can be calculated. Armed with this information and the discussion in the two previous chapters, the most probable interpretation of the event(s) can be made. It will also be appropriate to consider the implications if the event is due to a source other than the most probable one. It will be very important to check the self-consistency of the various possible interpretations. This in itself is an important source of information. As an example, if an event is observed with a

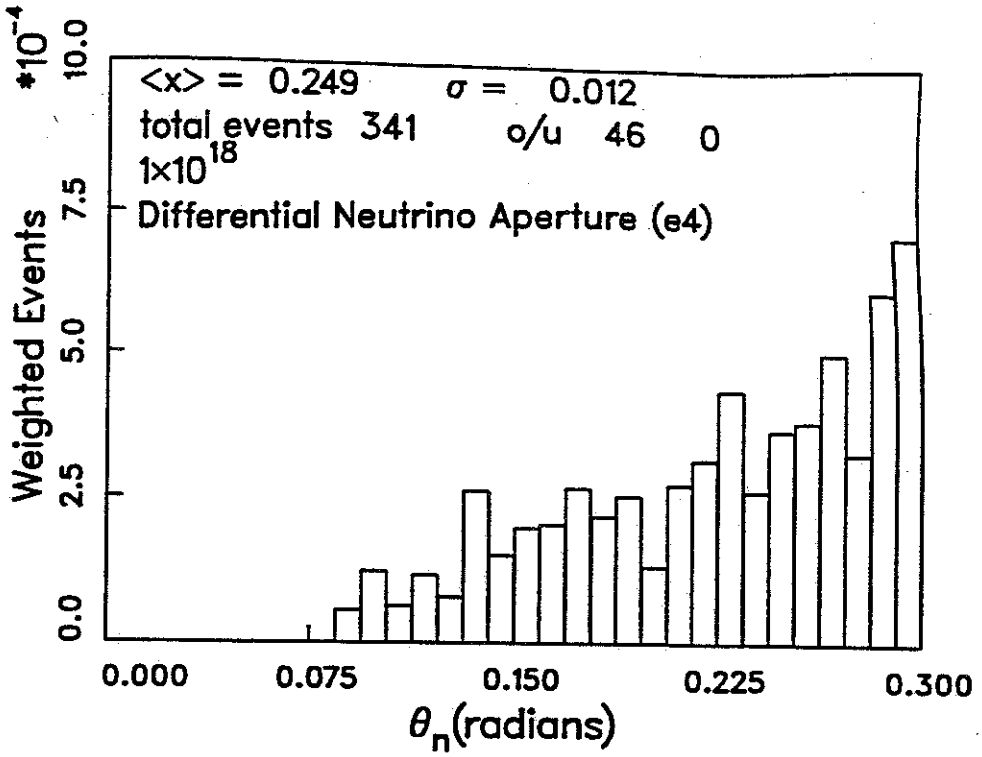


Figure 8.1. Differential aperture for detection of neutrino initiated deeply penetrating EAS as a function of $\theta_n$

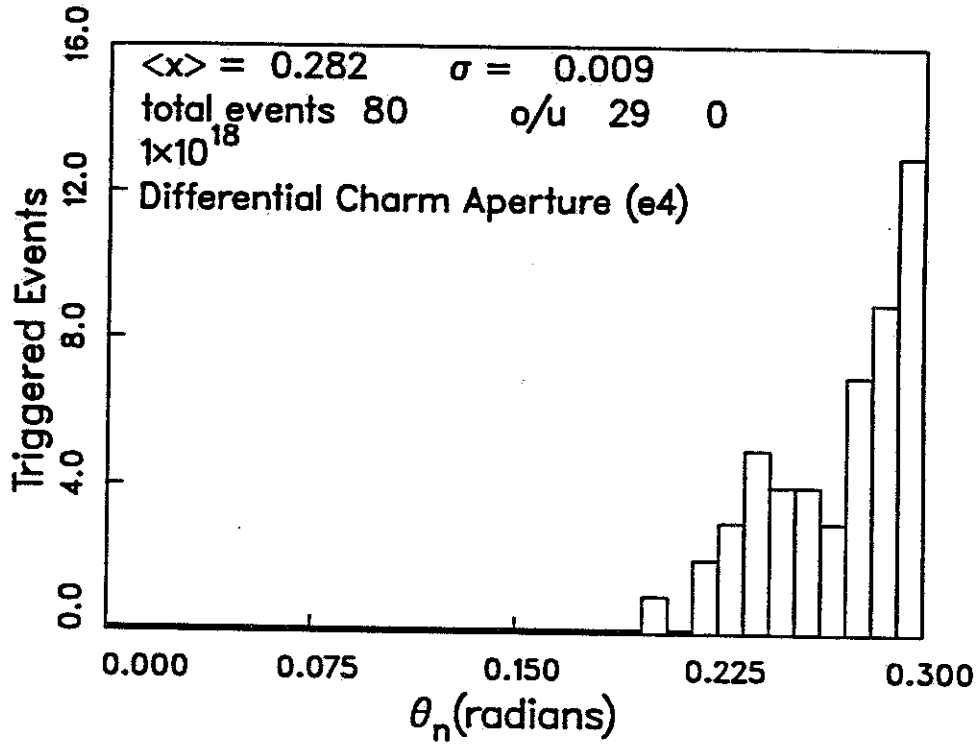


Figure 8.2. Differential aperture for detection of charm matter initiated deeply penetrating EAS as a function of $\theta_n$

$\theta_n$ of 17.5° then it is most plausible in the current view of the possible sources to ascribe it to a deeply penetrating charm particle. If this is true then there should also be a number of similiar events whose $\theta_n$ is slightly greater that 18°. If these almost-candidate events do not occur in the data set, then there is a potential lack of self-consistency. Perhaps such an event would be more plausible when viewed as a neutrino event.

Issues such as these will require a careful probabilistic treatment in the event that a deeply penetrating event is seen.

# CHAPTER 9

# SUMMARY

In summary, this dissertation describes the search for deeply penetrating events in EAS initiated by EHE cosmic rays. Fundamental to this search is the design of a robust a priori signature of such an event. This was accomplished by identifying an essential characteristic of events which are convincingly not due to standard hadron initiated EAS. The resulting signature of a deeply penetrating event is stated as follows: *Candidate deeply penetrating events are those whose $\theta_n$ is less than 18°.* In the process of verifying this criterion, significant modifications in the detector simulator were needed. These modifications were required to achieve consistency bwteen the Monte Carlo output and the real data. A search of the monocular FE data set spanning $2 \cdot 10^7$s of detector on-time yielded no events that met the criterion for candidate events.

The implications of the nonobservation of deeply penetrating events was examined in the context of predicted fluxes of astrophysical neutrinos as well as models of charm production in EHE hadronic interactions. Models of astrophysical neutrino flux due to Hill and Schramm [58] and Stecker *et al.*[88] were evaluated. The neutrino flux due to the interaction of EHE cosmic rays with the 2.7° microwave background as calculated by Hill and Schramm is completely consistent with the nonobservation of events reported here. The nonobservation of deep events is also consistent with the neutrino flux from AGN's predicted by Stecker *et al.*

The characteristics of charm production at EHE energies ($\sqrt{s} = 15$TeV) were extrapolated from lower energies and used to model charm production in EHE EAS. The nonobservation of deep events was examined in the context of a variety of charm

production scenarios. Even for the most extreme choices of charm production and interaction parameters no deep events were predicted to occur in the FE data set. This is consistent with the result obtained.

The overall conclusion is that the nonobservation of candidate deeply penetrating events is completely consistent with all proposed mechanisms for the production of such events. It does not appear that any proposed models can be ruled out on the basis of this study.

For the future, there is room for some hope that deeply penetrating events may be observed when the HIRES detector is completed. This improved version of the FE experiment will have a substantially enhanced aperture for deeply penetrating events. In addition, the improved angular resolution of the instrument may make effective searches for upward and downward going neutrino events possible.

# APPENDIX A

# REPRODUCTION OF RESULTS

In the interest of facilitating the possible recalculation of these results, large batch files have been created. These batch files can be submitted to the system and run in the background. In some cases it may take days to complete the job. An important consideration is the amount of available disk space. I have tried to be efficient in the coding process the number of events that are generated to accurately model the response of the Fly's Eye to rare events and geometries is enourmous. 40 Mb files were not uncommon in this process. I will not describe any of the anaysis code and will rely on documentation in the code to lead future users through the algorithms.

To recalculate the expected neutrino events from the model of Hill and Schramm as well as that of Stecker *et al.* the first step is to locate the directory named /u/emerson/thesis/ndown. In this directory is an executable file called doneutall. As the name implies, this batch file does it all over a period of days. The output of this batch file will be found in the directory ...ndown/aperture in a file called ecalclogall. This file contains the expected events as a function of $\Xi$ from the model of Hill and Schramm and the expected events from the AGN model of Stecker *et al.*. If these models change or modification is desired the routine etcalc.f in /u/emerson/thesis/expected will need to be suitibly modified. For more specifics of the processing pipeline, one should refer to the many batch jobs contained in doneutall. The various ploting routines that might be of use are found in the appropriate directories with names that are indicative of their purpose.

The reproduction of the charm results is a bit less smooth. The process begins by moving to the /u/emerson/thesis/charm directory and linking the desired charm elasticity distribution to elast.dat. As an example, the results presented in this dissertation linked elast.11.dat to elast.dat to model charm propagation with a mean elasticity of .1. Once the desired distribution has been selected, then charmmc must be recompiled. After recompiling charmmc then the process shifts to the .../charm/analysis directory where the innocuous batch file called doallcharm resides. This file is then submitted to the system in a disk system with more than 50 Mb of free space. It may take as long as 5 days for this job to complete the task of determining the trigger efficiencies. When this task is completed, the next step is to execute the file called maketeffdat which uses an awk script to sort through the outputs from doallcharm and extract the trigger efficiencies in a useful format. The output of maketeffdat is a file teff.dat which is concatenated with other files using the maketeffblock command to produce a file called teffdata.f. Once again it is time to change directories to /u/emerson/thesis/charm/expected. In this directory the teffdata.f file must be compiled into the cecalc program. The final step is to execute the hardcalc and softcalc files that produce plots of the expected number of charm events for the different $x_F$ models as seen in Chapter 7.

The last task that may need to be reproduced is the selection of the $\theta_n$ cut. This was accomplished by running 100 times the number of cosmic rays expected in the current operating lifetime of the detector through the standard steruhcr simulator and examining in detail those events in the tail of the $\theta_n$ distribution. This may be accomplished by moving to the /u/emerson/thesis/ndown/thetancut directory. In this directory are three executable files called runcutap? where the ? is replaced by the detector epoch of interest. The data files output by this batch file must be concatenated by hand and a line count performed. The first entry in the file must be the number of lines in the file. After this global data file is created, typically called

cue?all.dat, the contents may be usefully plotted with plotallcu?. Only the tail of the $\theta_n$ distribution is contained in these data files due to disk space limitations.

# APPENDIX B

# MONTE CARLO

The principal modifications to the detector Monte Carlo will be documented here without explicitly presenting the code changes. Previous versions of the code may, in some cases, be found in the directory /l/fdat/source/mc/stev2.

The first important change was to include the 3-tube local coincidence in the ring 5 mirrors into the lctest subroutine. This modification has already been made in the group version of the lctest code. The specific implementation of this change is slightly different in my local version, found in /u/emerson/uhcr, but the effect is identical.

The other significant modification was to the attenn subroutine. This routine calculates the attennuation of light as it passes through the atmosphere due to both aerosol (Mie) scattering and Rayleigh scattering. The model of the distribution of atmospheric aerosols was rewritten to roughly conform to a more recent model of desert aerosols due to Spinhirne *et al.*[85]. The modified version of attenn is called attenn1 and the calls to attenn were appropriately changed throughout the steruhcr code. There several important features in this new model. A mixing layer with constant extinction coefficient lies at the bottom of the atmosphere. The thickness of this mixing layer is adjustable as needed. Data indicate that the mixing layer is between 500 m and 2000 m in thickness. Above the mixing layer, an exponential model of aerosol concentration is used. The scale height of the aerosols is a controllable parameter of the model. Above the troposphere, the aerosol extinction length is taken to be constant. Measurements actually indicate an increase in the extinction length up to altitudes of 20 km but the effects of

taking it to be constant are negligible. The height of the tropopause, which varies seasonally, is an important parameter of the model. In addition, the model contains the potential of including a layer of clouds with arbitrary extinction length at any desired altitude. For the purposes of this dissertation no such cloud layer was used.

It is important to note that the subroutine for calculating the scattering of Čerenkov light, aerp, contains its own model of atmospheric aerosols, which was modified to be consistent with the attenn1 subroutine.

The remaining modifications to the code come under the general heading of updates to the data structures. It was found that the noise generation routine was based on 2 photoelectrons/ns as opposed to .2 photoelectrons/ns which is the most recent measured value. The noise routine was updated to reflect this more current number. The quantum efficiency of the PMTs as a function of wavelength is a factor that affects a variety of calculations in many subroutines. These data statements were updated to relect the most recent measurements. The net effect of this change was negligible for the events studied in this dissertation. Recent work by Luo [68] suggests that the dependence of the intensity of the scattered Čerenkov on the scattering direction may be different than that currently in use. The proposed change is a result of assuming a different size distribution of the aerosols. Luo found that a lognormal size distribution provided a better fit to the scattering data from laser shots than the currently used power law distribution. This change was implemented in the cherlp1 subroutine where intensity of the scattered Čerenkov light is calculated.

# REFERENCES


[1] M. Aguilar-Benitez *et al.*, Phys. Lett. **B123**, 98, (1983)

[2] M. Aguilar-Benitez *et al.*, Z. Phys. C, **31**, 491, (1986)

[3] R. Ammar *et al.*, Phys. Rev. Lett., **61**, 2185, (1988)

[4] R.M. Baltrusaitis *et al.*, Ap. J., **281**, L9, (1984)

[5] R.M. Baltrusaitis *et al.*Phys. Rev. Lett., **52**, 1380, (1984)

[6] R.M. Baltrusaitis *et al.*, Phys. Rev. Lett., **54**, 1875, (1985)

[7] R.M. Baltrusaitis *et al.*, Phys. Rev., **D31**, 2192, (1985)

[8] R.M. Baltrusaitis *et al.*, Nucl. Inst. Meth. Phys. Res., **A240**, 410, (1985)

[9] V. Barger *et al.*, Phys. Rev. **D25**, 112, (1982)

[10] A.R. Bell, Mon. Not. R. Astrophys. Soc.,**182**, 147, (1978)

[11] E.L. Berger *et al.*, Nucl. Phys. B, **286**, 704, (1987)

[12] G. Bertsch *et al.*, Phys. Rev. Lett., **47**, 297, (1981)

[13] P.L. Biermann and P.A. Strittmatter, Ap. J., **322**, 643, (1987)

[14] J.D. Bjorken and L.D. McLarren, Phys. Rev. **D20**, 2353, (1979)

[15] R.D. Blandford and J.P. Ostriker, Ap. J. Lett., **221**, L29, (1987)

[16] Brasil-Japan Group, Proc. 15th ICRC (Plovdiv), **7**, 208, (1977)

[17] S.J. Brodsky and C. Peterson, Phys. Rev. D, **23**, 2745, (1981)

[18] S.J. Brodsky and P. Hoyer, Phys. Rev. Lett., **63**, 1566, (1989)

[19] A.N. Bunner, Ph.D. Thesis, Cornell University, Ithaca, NY, (1967)

[20] T.H. Burnett *et al.*, Ap. J., **349**, L25, (1990)

[21] G.L. Cassiday, Ann. Rev. Nucl. Part. Sci., **35**, 321, (1985)

[22] G.L. Cassiday *et al.*, Proc. 21st ICRC (Adelaide), **3**, 163, (1990)

[23] G.L. Cassiday *et al.*, Phys. Rev. Lett., **62**, 383, (1989)

[24] G.L. Cassiday *et al.*, Ap. J., **356**, 669, (1990)

[25] G.L. Cassiday *et al.*, Proc. 21st ICRC (Adelaide), 4, 282, (1990)

[26] G. Chanmugam and K. Brecher, Nature, **313**, 767, (1985)

[27] P. Chauvat *et al.*, Phys. Lett. **B199**, 304, (1987)

[28] K.S. Cheng and M.A. Ruderman, Ap. J., **337**, L77, (1989)

[29] A. Chodos and H. Nadeau, Phys. Rev. **D33**, 1450, (1986)

[30] H. Cobbaert *et al.*, Phys. Lett., **B191**, 456, (1987)

[31] H. Cobbaert *et al.*, Phys. Lett., **B206**, 546, (1988)

[32] S.A. Colgate, Proc. 18th ICRC (Bangelore), **2**, 230, (1983)

[33] J.J. Condon, Ap. J., **327**, 643, (1987)

[34] R. Cooper *et al.*, *Astrophysical Aspects of the Most Energetic Cosmic Rays* (World Scientific, Singapore, 1991), 34

[35] R. Cowsil and L. Wilson, Proc. 13th ICRC, **1**, 500, (1973)

[36] G. Cunningham *et al.*, Ap. J., **236**, L71, (1980)

[37] B. D'Almagne *1988 Int. Symp. on the Production and Decay of Heavy Flavors*, pp 445, AIP Press (1988)

[38] C. Detar, private communication

[39] J.S. Dunlop and J.A. Peacock, Mon. Not. R. Astrophys. Soc., **247**, 19,(1990)

[40] J. Donoghue and E. Golowich, Phys. Rev. D, **15**, 3421, (1977)

[41] M.E. Duffy *et al.*, Phys. Rev. Lett., **55**, 1816, (1985)

[42] E. Fermi, Physical Review, **75**, 1169, (1949)

[43] H.G. Fisher and W.M. Geist, Z. Phys. C, **19**, 159, (1983)

[44] T.K. Gaisser A.K. Harding, and T. Stanev, Nature, **329**, 314, (1987)

[45] T.K. Gaisser, A.K. Harding, and T. Stanev, Ap. J., **345**, 423, (1989)

[46] T.K. Gaisser, *Cosmic Rays and Particle Physics*, Cambridge University Press, (1990)

[47] T.K. Gaisser, Proc. 22nd ICRC (Dublin), **4**, 413, (1991)

[48] M. Giler *et al.*J. Phys. G **6**, 1561 (1980)

[49] M.L. Good and W.D. Walker, Physical Rev., **120**, 1857, (1960)

[50] K.D. Green, Ph.D. Thesis, University of Utah. (1992)

[51] K. Greisen, Phys. Rev. Lett., **16**, 748, (1966)

[52] J.E. Gunn and J.P. Ostriker, Phys. Rev. Lett., **22**, 728, (1969)

[53] M. Gupta and W.R. Webber, Ap. J., **340**, 1124, (1989)

[54] G. Gustafson and C. Peterson, Phys. Lett., **B67**, 81, (1977)

[55] P. Hamill *et al.*, J. Atmos. Sci., **34**, 1104, (1977)

[56] A.M. Hillas Can. J. Phys. **46**, S623 (1968)

[57] A.M. Hillas, J. Phys. G.: Nucl. Phys., **8**, 1461, (1982)

[58] C.T. Hill and D.N. Schramm, Phys. Rev., **D31**, 564, (1985)

[59] *Proposal to Construct a HiRes Detector* University of Utah Cosmic Ray Group

[60] J.E. Horvath and O.G. Benvenuto, Phys. Rev. **D41**, 3548, (1990)

[61] J. Irion *et al.*, Phys. Lett., **B99**, 495, (1981)

[62] J.R. Jokipii and G. Morfill, Ap. J., **312**, 170, (1987)

[63] A. Khodjamirian, Proc. 20th ICRC (Moscow), **6**, 158, (1987)

[64] T. Kifune, Proc. 21st ICRC (Adelaide), **11**, 75, (1990)

[65] H. Krimm, Ph.D. Thesis, The University of Chicago, (1991)

[66] M.A. Lawrence *et al.*, Proc. 21st ICRC (Adelaide), **3**, 159, (1989)

[67] M.S. Longair, Mon. Not. R. Astrophys. Soc., **133**, 421, (1966)

[68] S.M. Luo, Ph.D. Thesis, University of Utah, (1992)

[69] J. Matthews *et al.*, Ap. J., **375**, 202 (1991)

[70] W.H. Matthaeus *et al.*, Phys. Rev. Lett., **53**, 1449, (1984)

[71] P. Mazzanti and S. Wada, Phys. Rev. D, **26**, 602, (1982)

[72] L. McLerran and L. Stodolsky, Phys. Lett. **B109**, 485, (1982)

[73] M. Garcia-Munoz, G.M. Mason, and J.A. Simpson, Ap. J., **217**, 859, (1977)

[74] P. Nason *et al.*, Nucl. Phys. **B327**, 49, (1989)

[75] C.E. Navia *et al.*, Proc. 21st ICRC (Adelaide), **8**, 51, (1990)

[76] R. Odorico, Phys. Lett. B, **107**, 231, (1981)

[77] J.P. Ostriker *et al.*, Physics Lett., **B180**, 231, (1986)

[78] A.A. Penzias and R.W. Wilson, Ap. J., **142**, 419, (1965)

[79] B. Peters and N.J. Westergaard, Ap. Space Sci., **48**, 21, (1977)

[80] R.J. Protheroe, Proc. 20th ICRC (Moscow), **8**, 21, (1987)

[81] J.L. Puget, F.W. Stecker, and J.H. Bredekamp, Ap. J., **205**, 638, (1976)

[82] C. Quigg, M.H. Reno, and T.P. Walker, Phys. Rev. Lett., **57**, 774, (1986)

[83] M. Schmidt, in *Stars and Stellar Systems*, ed. G. Kuiper, University of Chicago Press, (1975), Vol. IX

[84] P. Skubic *et al.*, Phys. Rev. D, **18**, 3115, (1978)

[85] J.D. Spinhirne *et al.*, J. Ap. Met.,**19**, 426, (1980)

[86] F.W. Stecker, Phys. Rev. Lett., **21**, 1016, (1968)

[87] F.W. Stecker, Ap. J. **228**, 919, (1979)

[88] F.W. Stecker *et al.*, Phys. Rev. Lett., **66**, 2697, (1991)

[89] A. Strong *et al.*J. Phys. A **7**, 120 (1974)

[90] S.P. Swordy *et al.*, Ap. J., **349**, 625, (1990)

[91] L.V. Volkova, Sov. J. Nucl. Phys., **31**, 784, (1980)

[92] J.V. Wall, T.J. Pearson, and M.S. Longair, Mon. Not. R. Astrophys. Soc., **193**, 683, (1980)

[93] E. Witten, Phys. Rev. **D30**, 272, (1984)

[94] G.T. Zatsepin and V.A. Kuz'min, JETP Lett., **4**, 78, (1966)